Ore Geology Reviews 89 (2017) 350–368

Contents lists available at ScienceDirect

Ore Geology Reviews

journal homepage: www.elsevier.com/locate/oregeo

Geochronology, geochemistry and Sr–Nd–Hf–S–Pb isotopes of the Early Cretaceous Taoxihu Sn deposit and related granitoids, SE China

Qing-He Yan [a,b], Sha-Sha Li [a,b], Zeng-Wang Qiu [a,b], He Wang [a,*], Xiao-Peng Wei [a,b], Pei-Li [a,b], Rui Dong [a,b], Xiao-Yu Zhang [a,b]

[a] CAS Key Laboratory of Mineralogy and Metallogeny, Guangzhou Institute of Geochemistry, Chinese Academy of Sciences, Guangzhou 510640, China
[b] University of Chinese Academy of Sciences, Beijing 100049, China

ARTICLE INFO

Article history:
Received 18 September 2016
Received in revised form 19 May 2017
Accepted 25 May 2017
Available online 29 May 2017

Keywords:
Taoxihu Sn polymetallic deposit
Zircon U–Pb dating
Molybdenite Re–Os dating
Fractionated I-type granite
Sr–Nd–Hf–S–Pb isotopes

ABSTRACT

The Taoxihu deposit (eastern Guangdong, SE China) is a newly discovered Sn polymetallic deposit. Zircon U-Pb dating yielded 141.8 ± 1.0 Ma for the Sn-bearing granite porphyry and 145.5 ± 1.6 Ma for the biotite granite batholith it intruded. The age of the granite porphyry is consistent (within error) with the molybdenite Re–Os isochron age (139.0 ± 1.1 Ma) of the Sn mineralization, indicating a temporal link between the two. Geochemical data show that the granite porphyry is weakly peraluminous, contain high Si, Na and K, low Fe, Mg, Ca and P, and relatively high Rb/Sr and low K/Rb values. The rocks are enriched in Rb, Th, U, K, and Pb and depleted in Ba, Sr, Ti and Eu, resembling highly fractionated I-type granites. They contain bulk rock initial $^{87}Sr/^{87}Sr$ of 0.707371–0.707730 and εNd(t) of −5.17 to −4.67, and zircon εHf(t) values from −6.67 to −2.32, with late Mesoproterozoic T_{DM2} ages for both Nd and Hf isotopes. This suggests that the granite porphyry was likely formed by the partial melting of the crustal basement of Mesoproterozoic overall residence age with minor mantle input.

$\delta^{34}S_{CDT}$ values of the Taoxihu chalcopyrite and pyrite range from 0.1 to 2.1‰ (average: 0.9‰), implying a dominantly magmatic sulfur source. The $^{206}Pb/^{204}Pb$, $^{207}Pb/^{204}Pb$ and $^{208}Pb/^{204}Pb$ ratios of the Taoxihu sulfide ores are 18.497–18.669, 15.642–15.673 and 38.764–38.934, respectively, indicating a mainly upper continental crustal lead source with minor mantle contribution. The highly fractionated and reduced (low calculated zircon Ce^{4+}/Ce^{3+} and Eu_N/Eu_N^* values) nature of the ore-forming granitic magma may have facilitated the Sn enrichment and played a key role in the Sn mineralization. We propose that the ore-forming fluids at Taoxihu were of magmatic-hydrothermal origin derived from the granite porphyry, and that both the granite porphyry and the Sn mineralization were likely formed in an extensional setting, possibly related to the subduction slab rollback of the Paleo-Pacific Plate.

1. Introduction

South China is a world-class W–Sn province, and the majority of the granite-related W–Sn polymetallic deposits are distributed in the Nanling fold belt, Youjiang basin, North Jiangxi area, and SE coastal magmatic belt (Hu and Zhou, 2012; Mao et al., 2013; Xu et al., 2016; Huang and Jiang, 2014). The mineralization is considered to be spatially and genetically associated with not only S-type, but also I- and A-type Late Mesozoic granites (Hua et al. 2005; Xu et al., 2016; Li et al., 2007c). Eastern Guangdong is tectonically located at the junction of the EW-trending Nanling fold belt and the NE-trending coastal magmatic belt (Fig. 1; Xu and Yue, 1999a), with over 50 Sn–W polymetallic deposits being discovered, e.g. Jinkeng, Tiandong, Sanjiaowo, Tashan, Changpu, Jishuimen, Xiling, Hopoao and Lianhuashan (Xu and Yue, 1999a; Liu et al., 2015a,b; Qiu et al., 2016, 2017a,b).

The recently discovered Taoxihu Sn polymetallic deposit is located in the Lianhuashan fault zone in eastern Guangdong. Little is known about the magmatic and mineralization ages, granite petrogenesis, metal, and fluid sources of the deposit and its related granites. Here, we present the first systematic study of the geology, zircon U–Pb and molybdenite Re–Os geochronology, geochemistry, and Sr–Nd–Hf–S–Pb isotopes of the mineralization-related granite porphyry at Taoxihu. We then discuss the petrogenesis of the granite porphyry and its implications for the Sn mineralization, as well as the Late Mesozoic regional geodynamics in South China.

* Corresponding author.
E-mail address: wanghe@gig.ac.cn (H. Wang).

http://dx.doi.org/10.1016/j.oregeorev.2017.05.026
0169-1368/

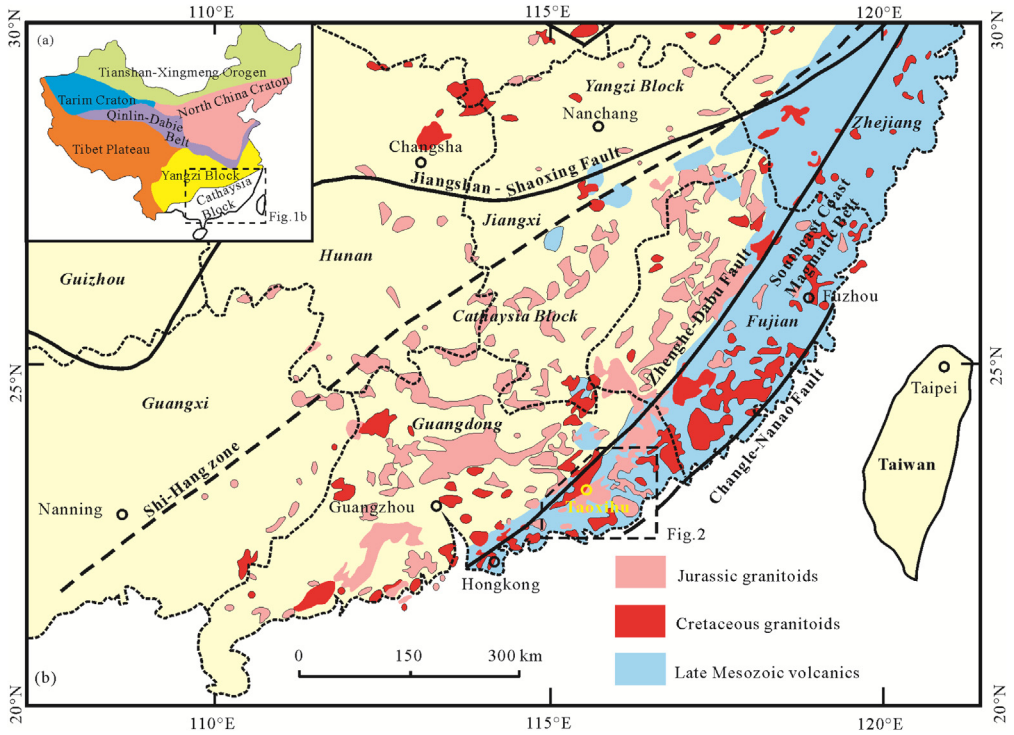

Fig. 1. (a) Tectonic map of China; (b) Simplified regional geologic map, showing the distribution of Mesozoic granitoids and volcanics in South China (modified after Zhou et al., 2006).

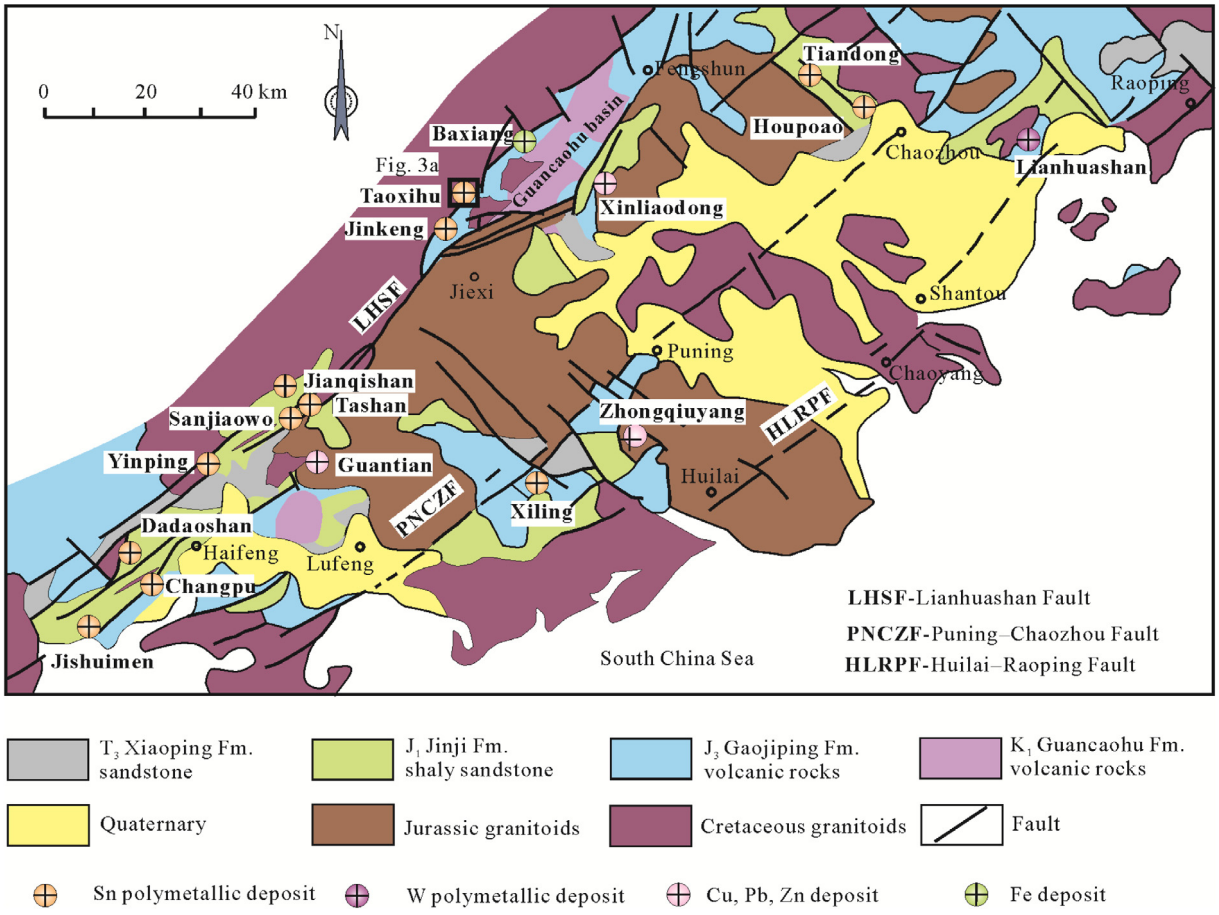

Fig. 2. Geologic map of eastern Guangdong (modified after Xu and Yue, 1999a).

2. Regional geology

Eastern Guangdong is located in the SE part of the Cathaysia Block. The regional geology is dominated by sedimentary rocks of the Upper Triassic Xiaoping and Lower Jurassic Jinji formations, volcanic rocks of the Upper Jurassic Gaojiping Formation, and the red bed and tuffaceous clastic sediments of the Lower Cretaceous Guancaohu Formation (Fig. 2; Xu and Yue, 1999a; Xu et al., 2000). NE- and NW-trending faults are the major structures in this region, with the former (i.e., the Lianhuashan, Puning–Chaozhou and Huilai–Raoping fault zones) controlling the emplacement of Mesozoic granitoids and their related ore deposits, e.g., those along the Jishuimen-Baxiang, Xiling–Houpoao and Zhongqiuyang–Lian huashan W–Sn belts (Fig. 2; Xu and Yue, 1999a; Qiu et al., 2016, 2017a,b). Middle Jurassic-Early Cretaceous granitoids are abundant in the region, and mainly comprise biotite granite, monzogranite, granodiorite, quartz porphyry, and granite porphyry. Voluminous coeval volcanic rocks (e.g., rhyolite, tuff, ignimbrite, and breccia) are also present along the regional faults, or inside rift basins such as the Early Cretaceous Guancaohu Basin (Qiu et al., 2017a). Previous research suggested that both the granitoids and volcanic rocks are transitional I-/S-type (Xu et al., 2000).

The regional Lianhuashan fault zone constitutes a low- to medium-pressure metamorphic belt in the study area, and contains strongly mylonitized and foliated rocks. The fault was active since the Early Jurassic (Qiu et al., 1991), and was associated with the regional volcanic eruption, granitoid intrusion and the related endogenic polymetallic deposits of the Jishuimen-Baxiang Sn polymetallic metallogenic belt. There are over 30 deposits discovered in this belt, including the Jinkeng, Taoxihu, Tashan, Dadaoshan, Changpu, Jishuimen Sn polymetallic deposits (Qiu et al., 2017a).

3. Deposit geology

The Taoxihu Sn deposit is located in the northeastern part of the Jishuimen-Baxiang Sn polymetallic metallogenic belt (Fig. 2). The exposed strata consist mainly of Upper Jurassic Gaojiping Formation (predominantly felsic volcanic lavas/volcaniclastic rocks

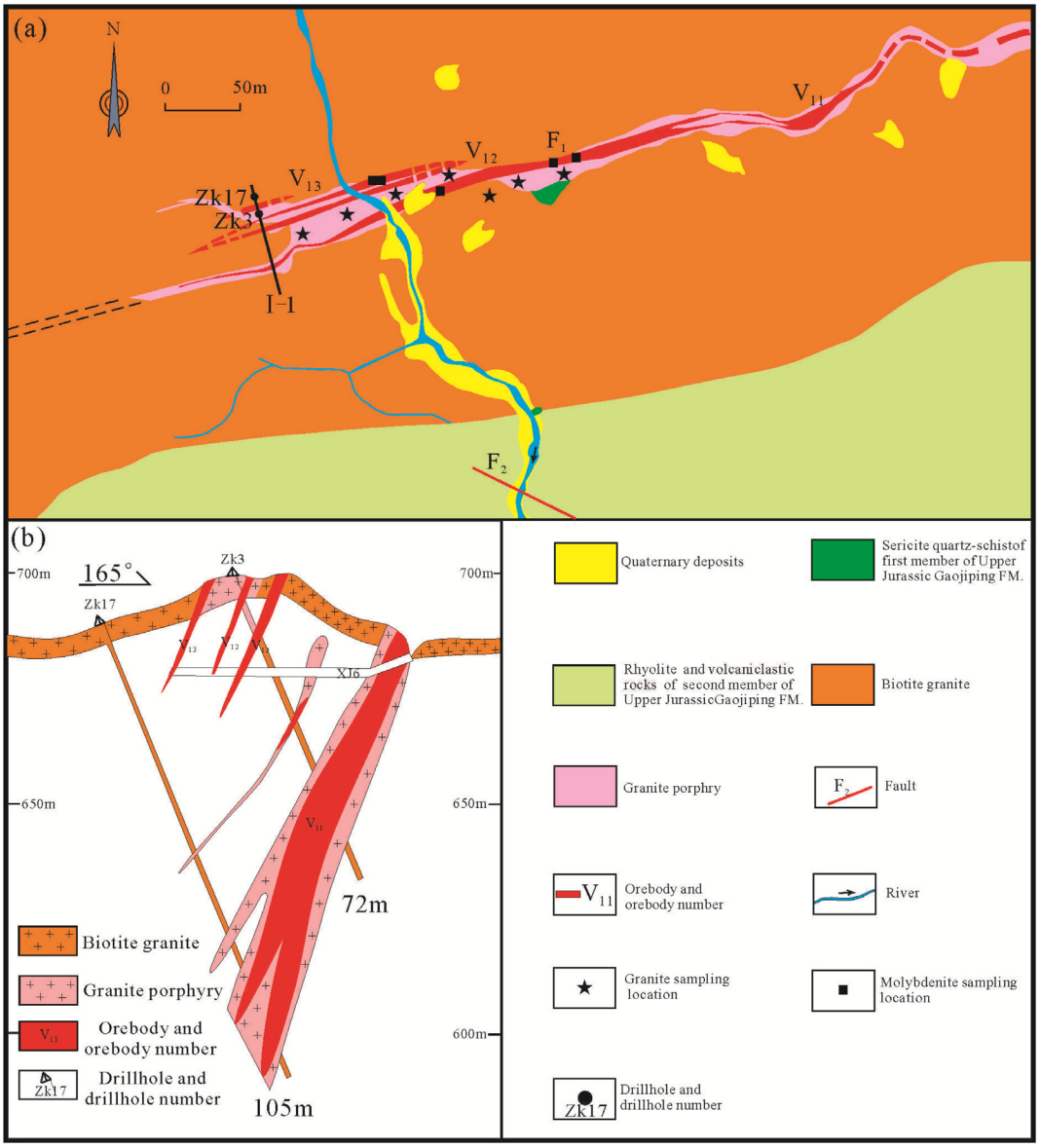

Fig. 3. (a) Geologic map of the Taoxihu Sn polymetallic deposit; (b) Geologic cross-section along Exploration Line No. I-1, showing the features of the Sn orebodies (modified after GNMGB, 2014).

interbedded with minor (meta)-siltstone) (Fig. 3a). These rock units generally crop out in a NE–SW orientation and dip to the SE between 35° and 55°. The NE and NW trending dominant structures controlled by the regional Lianhuashan Fault are well developed, of which the most important are the F_1 and F_2 faults (Fig. 3a). F_1 occurs in contact belt between the rocks in the exocontact zone and the granite porphyry (Fig. 3a).

Granitic rocks, which intruded the Gaojiping Formation, at Taoxihu they include a biotite granite batholith and its intruding associated granite porphyry dikes (Fig. 3a). The NE-trending granite porphyry dike extends for about 1 km and is 10–35 m wide. The biotite granite contains quartz (25–30%), K-feldspar (30–35%), plagioclase (27–30%) and biotite (2%) (Fig. 4a and c), whilst the granite porphyry dyke contains phenocrysts (30–40%) of quartz, K-feldspar, plagioclase and few biotite (Fig. 4b and d) with accessory zircon, monazite and apatite.

Until recently, three major ore veins and some minor parallel ones have been discovered at Taoxihu (Fig. 3). The orebodies (including the largest one: V_{11}) are mainly hosted in the granite porphyry (and its alteration zones), indicating a spatial relation between them. Orebody V_{11} is 350 m long, and extends up to 150 m deep at a dip angle of 35–75°. Its thickness is around 0.5–2.0 m (5.91 m max) (Fig. 3b). Major ore minerals in Taoxihu deposit include cassiterite and chalcopyrite, with an average grade of 0.52% Sn and 0.77% Cu for the whole deposit (GNMGB, 2014).

At Taoxihu, the mineralization styles are dominantly veinlet-disseminated and quartz vein (Fig. 5b–e). Major metal minerals include cassiterite, sphalerite, chalcopyrite and pyrite, with minor galena, arsenopyrite and molybdenite (Fig. 5f–i). Gangue minerals include quartz, plagioclase, fluorite, sericite, biotite, chlorite and garnet (Fig. 5f–h). Silicic, greisen, biotite, and fluorite alterations are found at Taoxihu (Fig. 5b–h), with the Sn mineralization closely related to intensive biotite alteration.

4. Sampling and analytical methods

Six representative fresh granite porphyry samples were collected from exploration trenches for the whole-rock geochemical, zircon U–Pb age, and Hf isotope analysis. Five molybdenite samples were collected for the Re–Os dating (Fig. 3a). Sulfides (pyrite and chalcopyrite) were collected for the S and Pb isotope analyses.

4.1. Whole-rock major and trace elements

Major and trace element concentrations were measured at the State Key Laboratory of Isotope Geochronology, Guangzhou Institute of Geochemistry, Chinese Academy of Sciences (GIGCAS). Major element concentrations (wt%) were determined on fused glasses, employing a Rigaku ZSX100e X-ray Fluorescence (XRF) spectrometer with an accuracy of around 1% for SiO_2, 5% for MnO and P_2O_5, and 2% for other major elements (Li et al., 2003a,b). Trace element concentrations were measured with a Perkin-Elmer Sciex ELAN 6000 Inductively Coupled Plasma–Mass Spectrometry (ICP–MS) at the GIGCAS, following the procedures outlined by Li et al. (2002). Analytical precision is generally better than 5% (Li et al., 2002).

4.2. Zircon LA–ICP–MS dating

Zircons were separated using conventional heavy liquid and magnetic methods, and then handpicked under a binocular microscope. The zircons grains were mounted in epoxy resin and polished. Cathodoluminescence (CL) images were taken with a JXA-8100 Electron Probe Microanalyzer (EPMA) with a Mono CL3 CL system at the GIGCAS to study the zircon internal structure, and to ensure the zircons chosen for the analysis are free of inclusions or cracks.

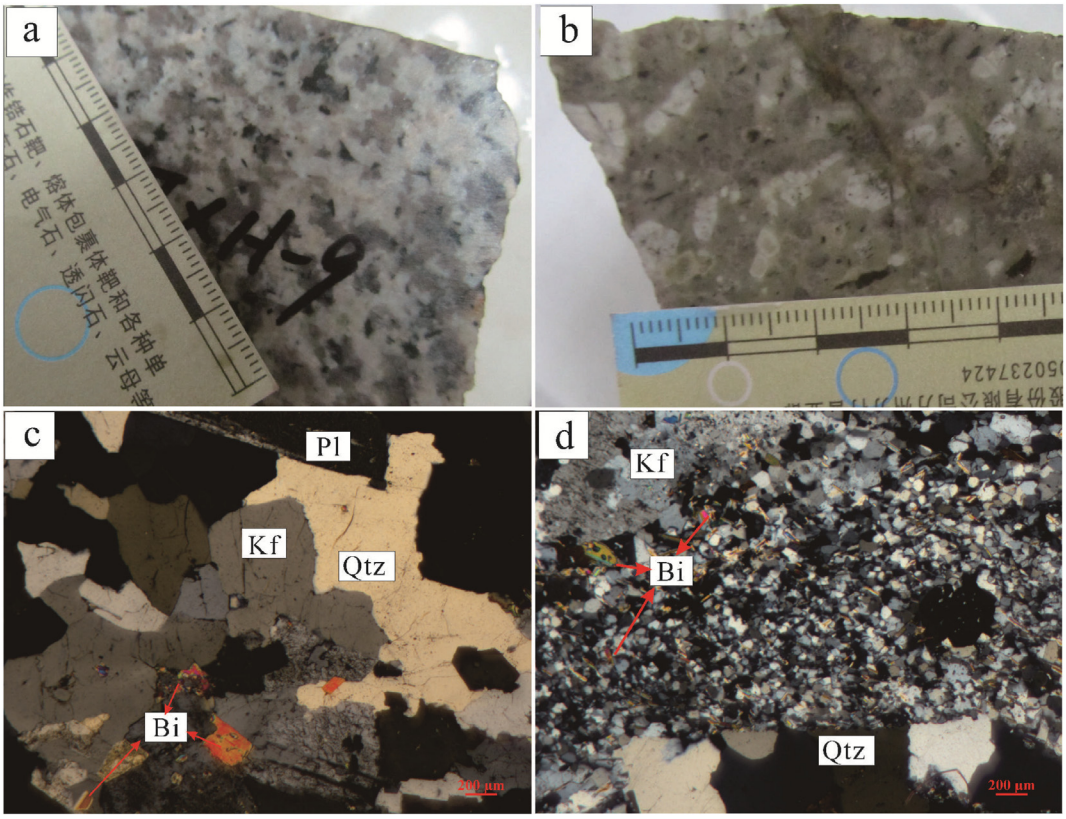

Fig. 4. (a), (b) Photograph and (c), (d) photomicrograph showing the biotite granite and granite porphyry at Taoxihu. Abbreviations: Q = quartz, Kf = K-feldspar, Pl = plagioclase, Bi = biotite.

LA–ICP–MS zircon U–Pb dating was carried out using an Agilent 7500a ICP–MS instrument coupled with a 193 nm wave laser microprobe at the State Key Laboratory of Isotope Geochronology and Geochemistry, GIGCAS. The analysis spot size was 31 μm, laser energy was 80 mJ and frequency was 10 Hz (with a 40 s ablation period). Uranium, Th, and Pb concentrations were calibrated by using ^{29}Si as an internal standard and NIST 610 glass as the reference standard. Zircon standard 91500 was used as an external standard and was analyzed once every five analyses, and zircon standard Temora was used for age calibration (^{206}Pb/^{238}U = 416.8 Ma; Black et al., 2003). Detailed analytical procedures used were similar to those described by Li et al. (2011). Offline selection and integration of background and analytical signals, and time-drift correction and quantitative calibration for U–Pb dating were undertaken using ICPMS DataCal 10.1 software (Liu et al., 2010). Common Pb was corrected following Andersen (2002), and the results and associated age calculations are shown in a concordant diagram constructed using ISOPLOT (V.3.0; Ludwig, 2003).

4.3. Molybdenite Re–Os isotopic dating

Five molybdenite samples from the Taoxihu Sn plymetallic deposit were crushed, separated, and sieved to obtain monomineralic molybdenite separates with purity >99%. The analysis was conducted at the Key Laboratory of Isotope Geochronology and Geochemistry, GIGCAS. Rhenium and Os concentrations and isotope compositions were determined using a Thermo Scientific X Series 2 ICP–MS using the chemical separation processes and analytical methods described by Sun et al. (2010). Uncertainties in spike calibrations, weighing of both spikes and samples, mass spectrometry measurement of isotope ratios, mass fractionation factors, and the ^{187}Re decay constant were all taken into account during these analyses (Sun et al., 2010).

4.4. Zircon Hf isotopes

The analysis was conducted using a Neptune Plus multi-collector (MC)–ICP–MS equipped with a RESOlution M-50 laser ablation system at the State Key Laboratory of Isotopic Geochemistry, GIGCAS. The Lu–Hf isotopic measurements were made on the same spots previously used for the U–Pb analysis. A laser repetition rate of 8 Hz at 80 mJ was used and the laser spot size was 45 μm. Zircon standard Penglai was used as a reference standard (Li et al., 2010), and the analytical procedures were as described by Wu et al. (2006). Isobaric interference of ^{176}Yb and ^{176}Lu on ^{176}Hf was corrected using ^{173}Yb and ^{175}Lu concentrations, and ^{176}Hf/^{177}Hf ratios were normalized to the ^{179}Hf/^{177}Hf value of 0.7325 using an exponential law for mass bias correction. Initial Hf isotope ratios were

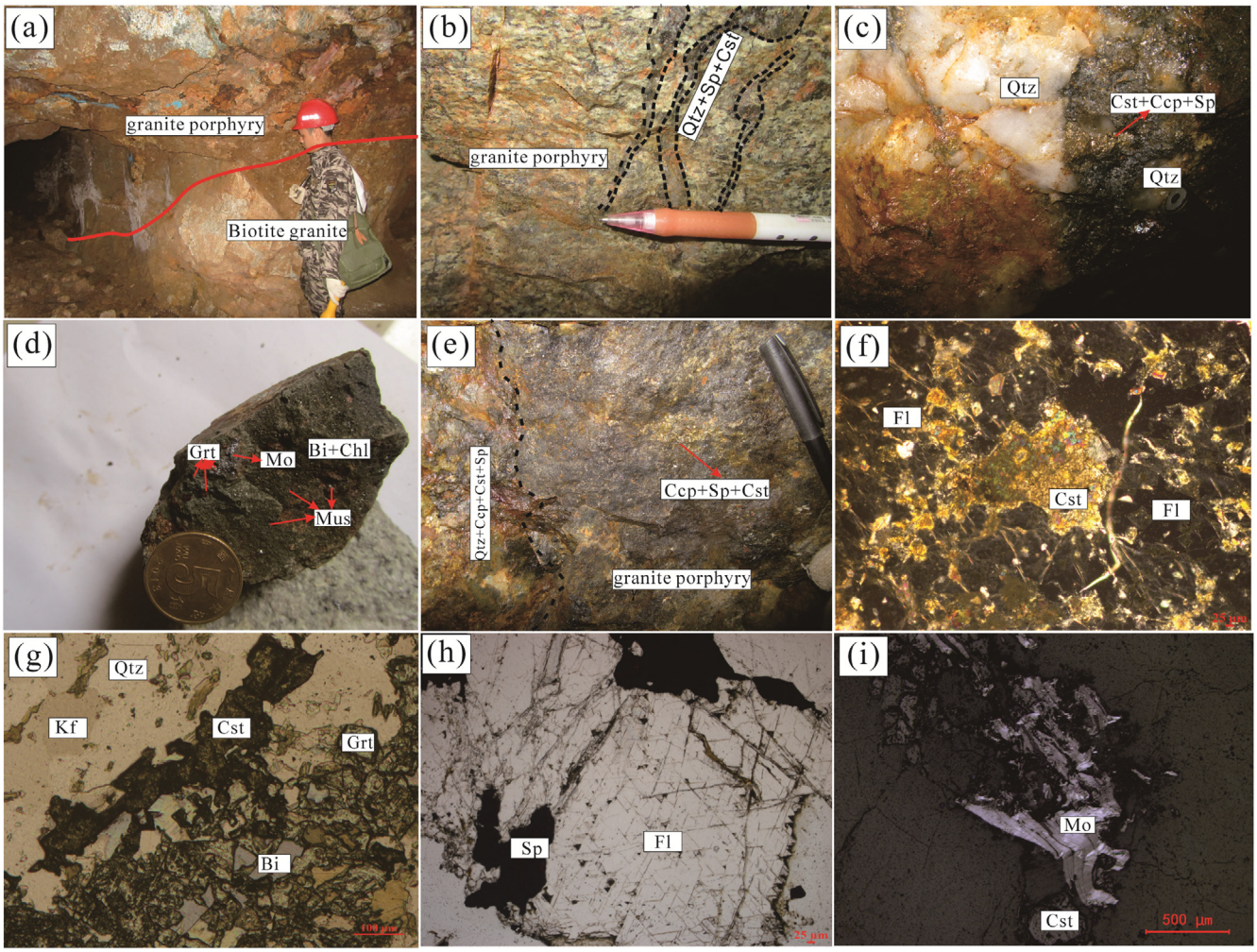

Fig. 5. Photographs and photomicrographs taken under (i) reflected light and (f–h) plane polarized light of the Taoxihu Sn mineralization. (a) Granite porphyry intruded biotite granite; (b) Veined mineralization in granite porphyry; (c) Quartz-cassiterite-sulfide vein; (d) Disseminated cassiterite-molybdenite ores; (e) Veined–disseminated sphalerite–chalcopyrite–cassiterite ores and quartz-cassiterite-sulfide veins in granite porphyry; (f) Cassiterite intergrown with fluorite. (g) Cassiterite intergrown with garnet and biotite; (h) Sphalerite intergrown with fluorite. (i) Cassiterite coexists with molybdenite. Abbreviations: Cst = cassiterite, Mo = molybdenite, Ccp = chalcopyrite, Sp = sphalerite, Qtz = quartz, Bi = biotite, Ms = muscovite, Fl = fluorite.

calculated using the Chondritic Uniform Reservoir (CHUR) value at the time of zircon crystallization and present-day $^{179}Hf/^{177}$ and $^{176}Lu/^{177}Hf$ ratios of chondrite and depleted mantle, respectively (Blichert-Toft and Albarede, 1997). Initial $^{176}Hf/^{177}Hf$ values were calculated based on a ^{176}Lu decay constant of 1.867×10^{-11}/a (Söderlund et al., 2004), and single-stage model Hf ages (T_{DM1}) were determined with reference to the depleted mantle using a present-day $^{176}Lu/^{177}Hf$ ratio of 0.28325 and a $^{176}Lu/^{177}Hf$ ratio of 0.0384 (Griffin et al., 2000). Two-stage model Hf ages (T_{DM2}) were computed using the $^{176}Lu/^{177}Hf$ value of 0.015 for the average continental crust (Griffin et al., 2002).

4.5. Whole-rock Sr–Nd–Pb isotopes

Powdered samples were first dissolved into Teflon bombs with a HF + HNO_3 mixture, and then Sr and REE were separated by using cation columns. Detailed sample preparation and chemical separation procedures were as described by Wei et al. (2002). Whole-rock Sr and Nd isotopic ratios were measured with a VG-354 MC–ICP–MS at GIGCAS, with the detailed analytical procedures as described by Liang et al. (2003). $^{86}Sr/^{88}Sr = 0.1194$ and $^{156}Nd/^{144}Nd = 0.7219$ were used for the mass fractionation corrections of the Sr and Nd isotopic ratios, respectively. The NBS987 and Shin Etsu JNdi-1 were used as the standards, which gave the measured $^{87}Sr/^{86}Sr = 0.710237 \pm 9$ (2σ) and $^{143}Nd/^{144}Nd = 0.512097 \pm 4$ (2σ), respectively. Lead was separated and purified by conventional cation-exchange technique with dilute HBr as an eluant. Repeated analyses of NBS 981 yielded average values of $^{206}Pb/^{204}Pb = 16.933 \pm 4$ (2σ), $^{207}Pb/^{204}Pb = 15.486 \pm 5$ (2σ) and $^{208}Pb/^{204}Pb = 36.682 \pm 2$ (2σ).

4.6. Sulfide S–Pb isotopes

The analysis for was performed at the Beijing Institute of Uranium Geology. The samples used were 200-mesh sulfides, and the analytical procedures were as described by Giesemann et al. (1994). The measurements were performed on a MAT-251 isotope ratio mass spectrometer, and the results were presented in δ^{34}SV-CDT‰ with an analytical precision of on a MAT-251 isotope ratio mass spectromettroilite (V-CDT) sulfide standard.

Sulfide Pb isotope compositions were analyzed on a GV IsoProbe-T thermal ionization mass spectrometer (TIMS) at the Beijing Institute of Uranium Geology. The analytical procedure involved dissolution of the samples using HF and $HClO_4$ in crucibles, followed by basic anion resin exchange to purify the lead. Analytical results for the standard NBS 981 are $^{208}Pb/^{204}Pb = 36.615 \pm 0.005$ (2σ), $^{207}Pb/^{204}Pb = 15.453 \pm 0.004$ (2σ), and $^{206}Pb/^{204}Pb = 16.934 \pm 0.005$ (2σ).

5. Analytical results

5.1. Major and trace elements

The granite porphyry contains high SiO_2 (74.91–76.15 wt%, mean = 75.47 wt%) and low Al_2O_3 (12.05–12.47 wt%,

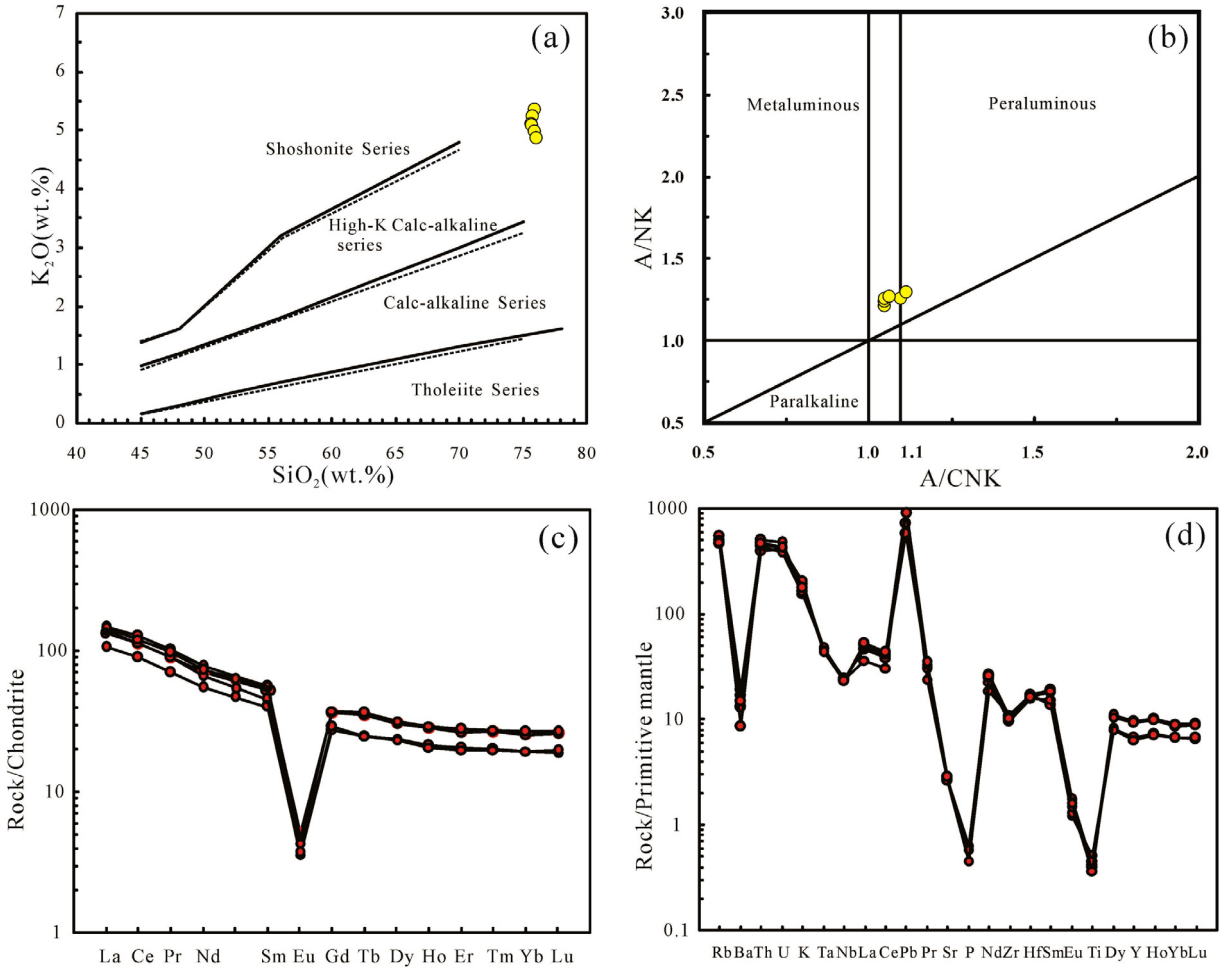

Fig. 6. Geochemistry of the Taoxihu granite porphyry: (a) K_2O vs. SiO_2 (Peccerillo and Taylor, 1976); (b) A/NK vs. A/CNK (Maniar and piccoli, 1989); (c) Chondrite-normalized REE; (d) primitive-mantle-normalized multi-element diagrams (normalizing values are from Sun and McDonough, 1989).

mean = 12.33 wt%). Total alkali concentrations range from 7.45 wt % to 8.38 wt% (mean = 7.87 wt%) with K_2O/Na_2O ratios of 1.72–2.74 (mean = 2.16). The rocks are peraluminous with A/CNK values (molar $Al_2O_3/(CaO + Na_2O + K_2O)$) of 1.06–1.12, and they contain low P_2O_5 (≤0.01 wt%), TiO_2 (0.08–0.11 wt%) and MgO (0.05–0.14 wt%). All the samples are classified as high-K calc-alkaline in the K_2O vs. SiO_2 diagram (Fig. 6a) and as weakly peraluminous in the A/NK (molar $Al_2O_3/(Na_2O + K_2O)$) vs. A/CNK diagram (Fig. 6b; Table 1).

Table 1
Major (wt%) and trace element (ppm) compositions of samples from the Taoxihu granite porphyry.

Samples	TXH-1	TXH-2	TXH-3	TXH-4	TXH-5	TXH-6
SiO_2	75.23	75.73	74.99	76.15	75.8	74.91
Al_2O_3	12.12	12.47	12.46	12.4	12.05	12.45
TiO_2	0.09	0.09	0.11	0.10	0.08	0.08
Fe_2O_3	2.37	1.83	2.59	2.11	2.61	2.21
MnO	0.08	0.09	0.13	0.07	0.16	0.13
MgO	0.14	0.11	0.08	0.06	0.05	0.06
CaO	0.68	0.79	0.85	0.81	0.93	0.92
Na_2O	2.18	2.24	2.61	2.74	2.67	2.62
K_2O	5.75	6.14	5.27	4.71	4.92	5.34
P_2O_5	0.01	0.01	0.01	0.01	0.01	0.01
L.O.I	0.66	0.57	0.55	0.47	0.45	0.62
Total	99.31	100.07	99.65	99.65	99.73	99.35
Na_2O/K_2O	0.38	0.37	0.50	0.58	0.54	0.49
A/CNK	1.10	1.06	1.08	1.12	1.06	1.06
A/NK	1.24	1.21	1.25	1.29	1.24	1.23
F	2410	3770	2700	3780	1710	3750
Sn	13	27	16	17	20	31
Sc	3.11	3.33	4.94	2.85	2.98	2.95
Ti	435.4	446.8	453	448	431	435
V	4.02	7.35	5.31	5.08	5.66	3.18
Cr	12.04	23.6	8.39	19	468	9.82
Mn	574	716	939	476	1151	914
Co	1.09	0.98	1.29	0.92	5.81	1.14
Ni	2.11	1.99	1.96	1.59	241	3.91
Cu	98.7	44.4	61.9	30.6	62.8	57.7
Zn	54.1	63.3	72.1	137	59.3	72.3
Ga	20.8	19.8	19.6	18.4	20.3	20.0
Ge	1.86	1.95	1.56	1.56	1.73	1.59
Rb	347	345	306	322	292	306
Sr	57.7	55.6	55.5	61.2	60.1	60.5
Zr	118	119	125	108	114	113
Nb	17.4	16.5	16.9	17.1	17.2	16.5
Cs	6.65	6.29	7.05	6.41	7.01	6.76
Ba	134	122	93.2	90.4	59.6	104
Hf	5.16	5.05	5.34	4.88	5.29	5.04
Ta	1.88	1.77	1.97	1.97	1.93	1.77
Pb	51.07	50.8	71.2	40.5	69.4	77.3
Th	40.8	39.5	33.3	37.4	42.9	39.3
U	9.08	8.72	8.74	8.03	9.90	8.88
La	31.6	35.01	25	32.9	34.2	36
Ce	69.5	77.7	54.5	68.5	74.1	77.2
Pr	8.61	9.64	6.67	8.48	9.21	9.55
Nd	32.9	36.11	25.5	30.8	34.2	34.9
Sm	8.08	8.51	6.1	6.78	8.42	8.39
Eu	0.30	0.27	0.21	0.22	0.25	0.27
Gd	7.52	7.55	5.58	5.93	7.67	7.59
Tb	1.30	1.32	0.92	0.93	1.35	1.32
Dy	7.89	7.64	6.05	5.93	8.06	7.77
Ho	1.62	1.62	1.21	1.17	1.66	1.61
Er	4.45	4.33	3.37	3.28	4.59	4.33
Tm	0.68	0.68	0.51	0.50	0.7	0.67
Yb	4.38	4.27	3.29	3.30	4.53	4.32
Lu	0.66	0.65	0.48	0.5	0.68	0.65
Y	43.38	44.14	30.7	29.2	43.7	42.8
ΣREE	179.5	195.3	139.4	169.2	189.6	194.6
LREE/HREE	5.30	5.96	5.51	6.86	5.48	5.89
Nb/Ta	9	9	9	9	9	9
Th/U	4	5	4	5	4	4
Rb/Sr	6.01	6.18	5.51	6.15	4.86	5.06
K/Rb	138	148	143	122	140	145
La_N/Yb_N	5.18	5.89	5.45	7.15	5.41	5.99
δEu	0.11	0.1	0.11	0.1	0.09	0.1
δCe	1.01	1.02	1.01	0.98	1.00	1.00
Zr + Nb + Ce + Y	248	257	227	223	248	250
Y + Nb	60.7	60.6	47.6	46.3	60.9	59.3
T_{Zr}(°C)	770	767	773	765	764	763

All the granite porphyry samples have similar REE patterns and distinct negative Eu anomalies ($Eu/Eu^* = 0.09 – 0.11$) (Fig. 6c). The rocks display moderate chondrite-normalized light REE (LREE)-enrichment patterns ($La_N/Yb_N = 5.18–7.15$), as well as large ion lithophile element (LILE, e.g., Rb, U, K and Pb) enrichments, extreme depletions in Ba, Sr, Ti and P, and slight depletions in Nb, Ta and Zr (Fig. 6d). Moreover, the rocks contain relatively high Rb/Sr (4.86–6.18, mean = 5.63) and low K/Rb values (122–148, mean = 139) (Table 1).

5.2. Zircon U–Pb geochronology

Zircons from the granite porphyry and biotite granite are dominantly euhedral to subhedral, light yellow in color, transparent and prismatic. The zircons are generally 80–200 μm in size and have length/width ratios of 2:1–3:1. Zircon CL imaging shows oscillatory zoning (Fig. 7a), which is indicative of a magmatic origin (Rubatto and Gebauer, 2000). As for the granite porphyry, among the 30 zircons analyzed (Table 2), 25 zircons (five discordant ones were discarded) contain a wide range of Th (131–1993 ppm) and U (87–1191 ppm) (Th/U ratios = 0.42–1.26; mean = 0.69). As for the biotite granite, the ten zircons analyzed (Table 2) also contain a wide range of Th (108–832 ppm) and U (215–1325 ppm U) (Th/U ratios = 0.41–1.12; mean = 0.67). High Th/U ratios (>0.1) is indicative of a magmatic origin (Belousova et al., 2002; Hoskin and Schaltegger, 2003; Wu and Zheng, 2004). Zircons from the granite porphyry (ca. 136.5–145.9 Ma) yielded a weighted mean $^{206}Pb/^{238}U$ age of 141.8 ± 1.0 Ma (MSWD = 0.42), whereas zircons from the biotite granite (ca. 141.9–149.8 Ma) yielded a weighted mean $^{206}Pb/^{238}U$ age of 145.5 ± 1.6 Ma (MSWD = 0.35) (Fig. 7a and b). These latest Jurassic-Early Cretaceous zircon U-Pb ages represent the emplacement ages of the biotite granite and granite porphyry.

5.3. Zircon Ce^{4+}/Ce^{3+} and Eu_N/Eu_N^* ratios

As the zircon La and Pr concentrations obtained are close to the minimum detection limits (Table 3), the Ce^{4+}/Ce^{3+} calculation method by Ballard et al. (2002) was adopted instead of the conventional one, i.e., $Ce_N/(La_N \times Pr_N)^{1/2}$. The Ce^{4+}/Ce^{3+} ratios of zircon were calculated on the basis of a lattice-strain model for mineral-melt partitioning of Ce^{4+} and Ce^{3+} cations. For the Ce^{4+}/Ce^{3+} calculation, whole-rock (sample TXH–1) trace element compositions were used as a proxy for the melt. As a result, the zircon Ce^{4+}/Ce^{3+} and Eu_N/Eu_N^* ratios of the Taoxihu granite porphyry were calculated to be 10.2–108.2 and 0.03–0.26, respectively.

5.4. Molybdenite Re–Os dating

Rhenium contents of the five Taoxihu molybdenite samples are of 0.0523–0.2311 ppm (average: 0.1616 ppm). The five consistent Re–Os model ages (ca. 138.62–139.78 Ma) yielded a weighted mean age of 139.06 ± 0.55 Ma (MSWD = 0.78) with good reproducibility (Fig. 8b). The data exhibit a good linear relation and yielded an isochron age of 139.0 ± 1.1 Ma (2σ, MSWD = 1.02) (Fig. 8a). The interception on the ^{187}Os axis is nearly zero within uncertainty, with an initial ^{187}Os value of 0.0001 ± 0.0016 ppm (Fig. 8a), indicating that the model age is reliable. The isochron age represents the timing of the Taoxihu molybdenite crystallization (Table 4).

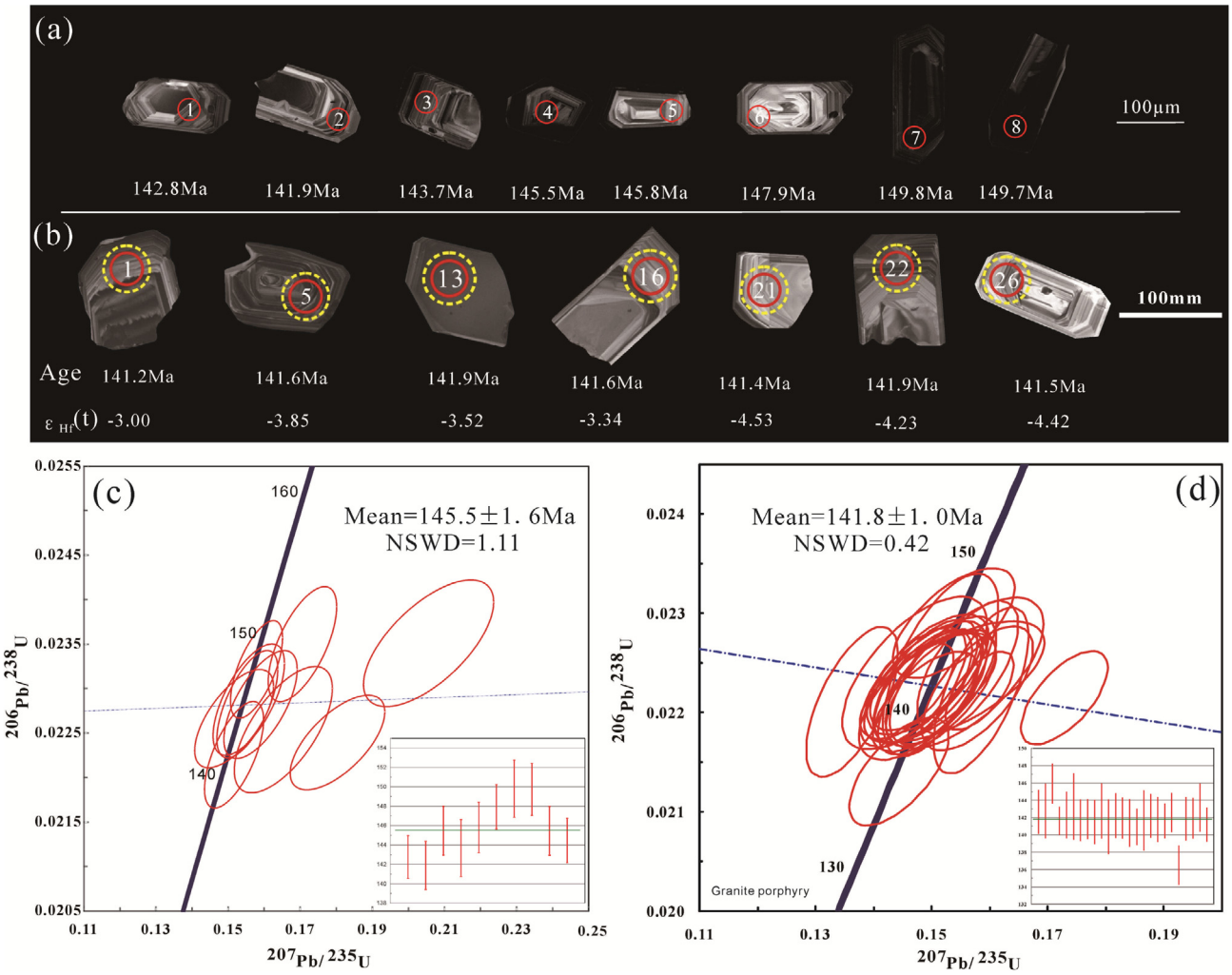

Fig. 7. Representative zircon CL images for the Taoxihu (a) biotite granite and (b) granite porphyry. The numbers denote analysis numbers, U–Pb ages and $\varepsilon_{Hf}(t)$ values, and the solid and dashed circles denote U–Pb and Hf analysis spots, respectively. Zircon U–Pb concordia diagrams and weighted mean age calculation for the Taoxihu (c) biotite granite and (d) granite porphyry.

5.5. Zircon Hf and whole-rock Sr–Nd–Pb isotopes

The 25 zircons analyzed from the granite porphyry (sample TXH–1) yielded varying $^{176}Hf/^{177}Hf$ ratios (0.2822501–0.282620), εHf(t) values (−6.67 to −2.32) and T_{DM2} ages (1343–1615 Ma) (Fig. 9a and b; Table 5).

The initial whole-rock Sr–Nd isotope compositions were calculated at 141.8 Ma (granite porphyry age). The calculated initial $^{87}Sr/^{86}Sr$ values fall into a narrow range (0.707371–0.707730) (Fig. 9; Table 6). The analysis yielded $^{143}Nd/^{144}Nd$ ratios of 0.512191–0.512216, with εNd(t) of −5.17 to −4.67 and corresponding TDM_2 of 1310–1349 Ma. The whole-rock $^{206}Pb/^{204}Pb$, $^{207}Pb/^{204}Pb$ and $^{208}Pb/^{204}Pb$ values are 18.657–18.682, 15.652–15.656 and 38.922–38.944, respectively (Table 7).

5.6. Sulfide Pb–S isotopes

Six Taoxihu sulfide (chalcopyrite and pyrite) grains (from three ore samples) have relatively homogeneous and low radiogenic Pb isotope compositions, with the $^{206}Pb/^{204}Pb$, $^{207}Pb/^{204}Pb$ and $^{208}Pb/^{204}Pb$ values being 18.497–18.669, 15.642–15.673 and 38.764–38.934, respectively (Fig. 11; Table 7).

The $\delta^{34}S_{VCDT}$ values of 6 sulfide (chalcopyrite and pyrite) separates from 3 ore samples in the Taoxihu Sn deposit range from 0.1 to 2.1‰, with an average of 0.9‰ (Fig. 12; Table 8).

6. Discussion

6.1. Timing of magmatism and mineralization

In this study, five molybdenite grains from the Taoxihu cassiterite–molybdenite ore mineral assemblage (Fig. 5i) yielded a weighted mean age of 139.06 ± 0.55 Ma and an isochron age of 139.0 ± 1.1 Ma. These Early Cretaceous mineralization ages are coeval with the granite porphyry emplacement (141.8 ± 1.0 Ma), suggests that the latter is likely Sn mineralization-related.

Compiling our new age data and the published ones, we suggest that the Sn–W ore-forming magmatism peaked at ca. 146–135 Ma and ca. 166–153 Ma, and that the major and minor Sn–W mineralization episodes occurred in ca. 145–135 Ma and ca. 161–153 Ma, respectively (Fig. 13; Table 9).

The Early Cretaceous W–Sn mineralization was closely related to coeval fractionated I- and A-type granites, such as the mineralization at Jinkeng, which is closely related the low oxidized and highly fractionated I type fine-grained granite (molybdenite Re–Os: 139.8 ± 5.0 Ma; zircon U–Pb: 141.1 ± 1.3 Ma; Qiu et al.,

Table 2
Zircon LA–ICP–MS U–Pb age data for samples from the Taoxihu granite porphyry and biotite granite.

LA-ICP-MS zircon U-Pb data for the Taoxihu granitoids																
Spot No.	Concentration (ppm)			Ratio	Isotopic Ratio						Age/Ma					
	Pb	Th	U	Th/U	$^{207}Pb/^{206}Pb$	1σ	$^{207}Pb/^{235}U$	1σ	$^{206}Pb/^{238}U$	1σ	$^{207}Pb/^{235}U$	1σ	$^{206}Pb/^{238}U$	1σ		
Sample TXH-1: Granite porphy (excluding spot TXH-1-3, TXH-1-4, TXH-1-6, TXH-1-10, TXH-1-17)																
TXH-1-1	21.62	436.34	749.30	0.58	0.05644	0.00167	0.17287	0.00493	0.02214	0.00031	161.9	4.3	141.2	2.0		
TXH-1-2	14.05	272.17	513.75	0.53	0.05161	0.00211	0.15852	0.00539	0.02222	0.00055	149.4	4.7	141.7	3.5		
TXH-1-5	57.08	1190.55	1993.41	0.60	0.05132	0.00119	0.15828	0.00387	0.02222	0.00026	149.2	3.4	141.6	1.6		
TXH-1-7	9.95	376.36	298.11	1.26	0.04902	0.00217	0.15382	0.00693	0.02290	0.00036	145.3	6.1	145.9	2.3		
TXH-1-8	7.15	205.90	250.87	0.82	0.05101	0.00286	0.15566	0.00897	0.02240	0.00050	146.9	7.9	142.8	3.2		
TXH-1-9	5.17	153.62	171.98	0.89	0.05009	0.00260	0.14936	0.00687	0.02238	0.00040	141.4	6.1	142.7	2.5		
TXH-1-11	10.42	214.92	376.31	0.57	0.05173	0.00198	0.15624	0.00572	0.02245	0.00044	147.4	5.0	143.1	2.8		
TXH-1-12	9.47	266.26	331.32	0.80	0.04929	0.00180	0.14855	0.00558	0.02226	0.00038	140.6	4.9	141.9	2.4		
TXH-1-13	9.93	266.02	344.05	0.77	0.04890	0.00208	0.14682	0.00605	0.02225	0.00040	139.1	5.4	141.9	2.5		
TXH-1-14	8.32	160.20	313.45	0.51	0.04961	0.00198	0.14440	0.00566	0.02140	0.00036	137.0	5.0	136.5	2.3		
TXH-1-15	13.11	268.56	462.53	0.58	0.04893	0.00214	0.14945	0.00661	0.02237	0.00036	141.4	5.8	142.6	2.3		
TXH-1-16	21.07	358.16	744.57	0.48	0.04765	0.00159	0.14609	0.00511	0.02221	0.00032	138.5	4.5	141.6	2.0		
TXH-1-18	13.47	229.02	490.90	0.47	0.05145	0.00192	0.15791	0.00630	0.02224	0.00041	148.9	5.5	141.8	2.6		
TXH-1-19	3.91	87.35	130.53	0.67	0.05072	0.00360	0.15357	0.01045	0.02230	0.00040	145.1	9.2	142.2	2.5		
TXH-1-20	13.89	461.31	435.15	1.06	0.04892	0.00196	0.14898	0.00600	0.02210	0.00033	141.0	5.3	140.9	2.1		
TXH-1-21	5.65	145.40	185.93	0.78	0.04855	0.00234	0.14931	0.00780	0.02218	0.00043	141.3	6.9	141.4	2.7		
TXH-1-22	12.56	219.96	463.68	0.47	0.04859	0.00189	0.14940	0.00621	0.02226	0.00038	141.4	5.5	141.9	2.4		
TXH-1-23	35.24	813.33	1255.52	0.65	0.04819	0.00161	0.14902	0.00587	0.02231	0.00041	141.0	5.2	142.2	2.6		
TXH-1-24	13.23	298.00	462.02	0.64	0.04513	0.00168	0.13634	0.00520	0.02210	0.00050	129.8	4.6	140.9	3.1		
TXH-1-25	7.93	235.33	263.66	0.89	0.04773	0.00253	0.14708	0.00820	0.02240	0.00051	139.3	7.3	142.8	3.2		
TXH-1-26	19.03	288.49	687.16	0.42	0.04881	0.00179	0.14965	0.00586	0.02219	0.00041	141.6	5.2	141.5	2.6		
TXH-1-27	6.56	184.95	213.93	0.86	0.04877	0.00239	0.14973	0.00749	0.02224	0.00036	141.7	6.6	141.8	2.3		
TXH-1-28	11.13	317.81	369.10	0.86	0.04919	0.00176	0.15086	0.00573	0.02223	0.00038	142.7	5.1	141.7	2.4		
TXH-1-29	18.18	357.06	565.12	0.63	0.04678	0.00242	0.15158	0.00653	0.02248	0.00061	143.3	5.8	143.3	3.8		
TXH-1-30	9.41	162.31	340.82	0.48	0.04956	0.00194	0.15202	0.00604	0.02232	0.00042	143.7	5.3	142.3	2.7		
Sample TXH-7: Biotite granite																
TXH-7-1	20.91	458.50	723.66	0.63	0.05756	0.00259	0.18033	0.00867	0.02239	0.00035	168.3	7.5	142.8	2.2		
TXH-7-2	11.81	319.50	388.07	0.82	0.04987	0.00190	0.15163	0.00541	0.02226	0.00040	143.4	4.8	141.9	2.5		
TXH-7-3	23.57	832.31	744.92	1.12	0.05289	0.00256	0.16531	0.00898	0.02254	0.00047	155.3	7.8	143.7	3.0		
TXH-7-4	17.98	273.50	663.28	0.41	0.04887	0.00148	0.15532	0.00558	0.02282	0.00040	146.6	4.9	145.5	2.5		
TXH-7-5	7.73	184.50	267.90	0.69	0.04925	0.00209	0.15571	0.00654	0.02288	0.00041	146.9	5.7	145.8	2.6		
TXH-7-6	36.21	619.68	1325.15	0.47	0.04891	0.00141	0.15786	0.00477	0.02322	0.00036	148.8	4.2	147.9	2.3		
TXH-7-7	18.72	356.27	645.95	0.55	0.06438	0.00453	0.20560	0.01192	0.02351	0.00047	189.9	10.0	149.8	3.0		
TXH-7-8	20.21	480.42	675.07	0.71	0.05282	0.00210	0.17060	0.00627	0.02350	0.00043	159.9	5.4	149.7	2.7		
TXH-7-9	10.61	276.24	355.89	0.78	0.05043	0.00195	0.15898	0.00672	0.02282	0.00040	149.8	5.9	145.5	2.5		
TXH-7-10	6.04	108.40	215.32	0.50	0.04887	0.00249	0.15166	0.00723	0.02266	0.00036	143.4	6.4	144.5	2.3		

Table 3
Zircon Lu–Hf isotopic compositions of samples from the Taoxihu granite porphyry.

Spot	La	Ce	Pr	Nd	Sm	Eu	Gd	Tb	Dy	Ho	Er	Tm	Yb	Lu	Hf	U	Th	Eu_N/Eu_N^*	Ce^{4+}/Ce^{3+}
TXH-1-1	0.18	14.43	0.14	1.70	4.19	0.17	28.64	10.28	122	46.48	202	40.23	355	71.1	12091	749	436	0.11	10.2
TXH-1-2	0.62	13.81	0.30	2.54	4.53	0.29	26.79	9.53	115	45.80	204	42.42	381	77.9	12741	514	272	0.17	10.3
TXH-1-5	0.01	12.28	0.14	3.97	11.09	0.12	72.60	25.82	305	115.28	495	97.57	849	163.0	13065	1993	1191	0.03	13.2
TXH-1-7	0.04	20.54	0.61	10.48	15.54	1.02	75.96	22.31	240	83.75	342	64.42	544	106.0	9631	298	376	0.17	13.5
TXH-1-8	0.03	12.42	0.20	3.28	6.39	0.32	31.42	9.64	104	37.20	153	30.06	302	51.1	10419	251	206	0.13	14.6
TXH-1-9	0.16	14.96	0.18	3.39	6.54	0.64	32.62	10.24	115	42.65	185	36.62	328	67.7	9683	172	154	0.26	14.9
TXH-1-11	0.00	11.77	0.05	1.03	3.40	0.13	21.72	7.72	89	33.18	142	29.10	245	48.9	12110	376	215	0.10	18.4
TXH-1-12	0.05	14.16	0.18	3.61	7.61	0.36	39.30	12.01	135	47.74	199	38.91	330	66.3	10580	331	266	0.13	18.4
TXH-1-13	5.82	30.26	2.43	12.23	7.69	0.29	34.88	10.57	116	41.97	173	33.45	289	57.6	10842	344	266	0.10	19.0
TXH-1-14	0.05	9.70	0.04	0.65	2.32	0.16	14.61	5.69	70	27.66	128	26.83	245	50.0	11867	313	160	0.18	28.6
TXH-1-15	0.05	12.53	0.10	1.67	3.99	0.15	26.55	8.95	107	40.11	171	34.37	301	59.4	11974	463	269	0.10	31.8
TXH-1-16	0.00	9.73	0.02	0.92	3.24	0.12	21.60	8.26	102	39.92	179	37.12	329	66.3	12918	745	358	0.10	32.1
TXH-1-18	8.39	35.43	4.36	25.82	12.28	0.14	28.33	7.91	82	28.80	124	25.14	222	44.5	12379	491	229	0.03	33.6
TXH-1-19	0.06	7.01	0.10	1.47	3.04	0.20	15.89	5.22	58	21.65	92	18.55	162	34.8	9595	131	87	0.17	35.9
TXH-1-20	0.03	17.56	0.32	5.41	9.89	0.34	47.95	14.36	155	54.12	222	42.31	360	71.4	10353	435	461	0.09	38.1
TXH-1-21	0.00	12.14	0.12	2.15	4.53	0.22	23.57	7.16	80	28.70	125	24.88	224	46.8	10249	186	145	0.13	49.8
TXH-1-22	0.00	7.93	0.02	0.65	2.40	0.06	17.03	6.13	75	28.59	127	26.13	231	47.4	12861	464	220	0.07	53.9
TXH-1-23	0.01	13.34	0.08	1.71	5.23	0.12	36.28	13.48	162	61.79	270	54.69	476	94.8	12819	1256	813	0.06	55.2
TXH-1-24	5.81	24.56	2.08	10.82	6.15	0.14	25.88	8.17	92	33.15	143	27.81	247	47.9	12271	462	298	0.06	58.9
TXH-1-25	0.70	13.98	0.49	6.18	8.71	0.42	40.97	12.44	135	46.79	195	36.84	317	63.1	10038	264	235	0.13	62.3
TXH-1-26	0.01	5.92	0.03	1.04	2.76	0.15	18.15	6.85	83	31.91	144	29.69	269	54.3	12407	687	288	0.14	62.9
TXH-1-27	0.09	6.86	0.18	3.33	6.11	0.29	29.26	8.75	95	34.68	144	27.63	245	49.1	9812	214	185	0.12	68.8
TXH-1-28	22.25	67.30	8.53	45.54	20.98	0.51	63.45	17.78	182	62.99	255	47.48	404	77.9	11215	369	318	0.06	72.5
TXH-1-29	0.00	13.75	0.08	1.72	4.00	0.17	26.67	9.05	106	40.14	175	34.71	305	61.1	12085	565	357	0.11	76.7
TXH-1-30	0.84	8.52	0.45	3.51	3.36	0.08	15.97	5.29	59	22.16	97	19.44	172	35.0	11342	341	162	0.07	108.2

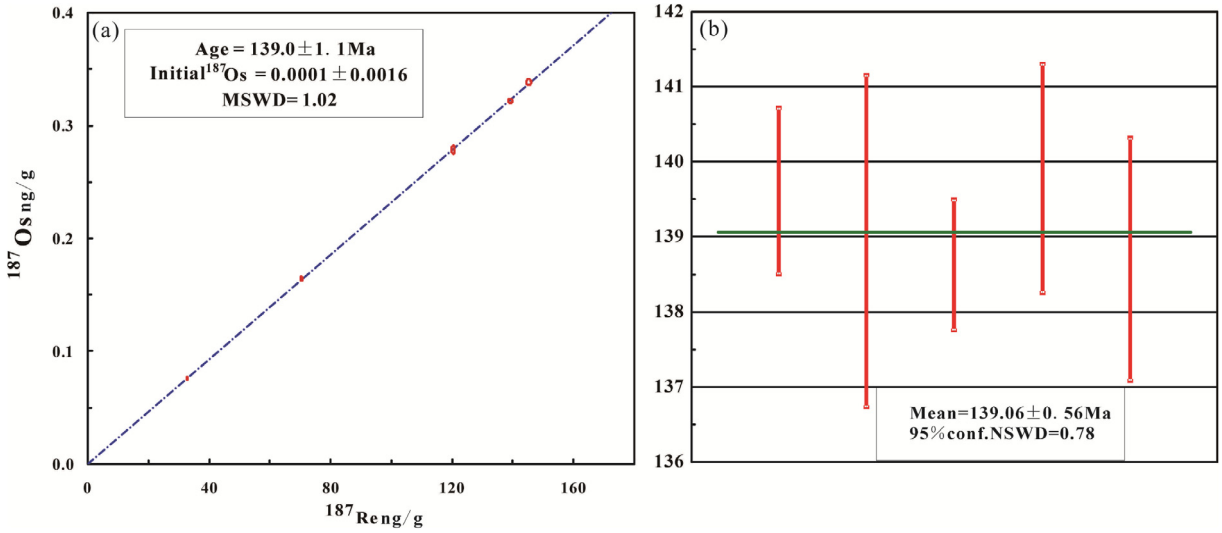

Fig. 8. (a) Molybdenite Re–Os isochron age and (b) weighted mean age for the Taoxihu deposit.

Table 4
LA–ICP–MS zircon trace element concentrations (ppm) and Ce^{4+}/Ce^{3+} and Eu_N/Eu_N^* ratios for the Taoxihu granite porphyry.

Sample	Weight/g	Re/μg g^{-1}		^{187}Re/μg g^{-1}		^{187}Os/ng g^{-1}		Age/Ma	
		Content	2σ	Content	2σ	Content	2σ	Model T	2σ
15TXH-1	0.5015	0.2311	0.0010	0.1452	0.0007	0.3382	0.0022	139.61	1.11
15TXH-2	0.5005	0.0523	0.0002	0.0329	0.0001	0.0761	0.0012	138.94	2.21
15TXH-3	0.5150	0.0519	0.0003	0.0326	0.0002	0.0757	0.0013	139.10	2.43
15TXH-4	0.5149	0.2213	0.0009	0.1391	0.0006	0.3216	0.0015	138.62	0.87
15TXH-5	0.5008	0.1120	0.0005	0.0704	0.0003	0.1641	0.0016	139.78	1.53

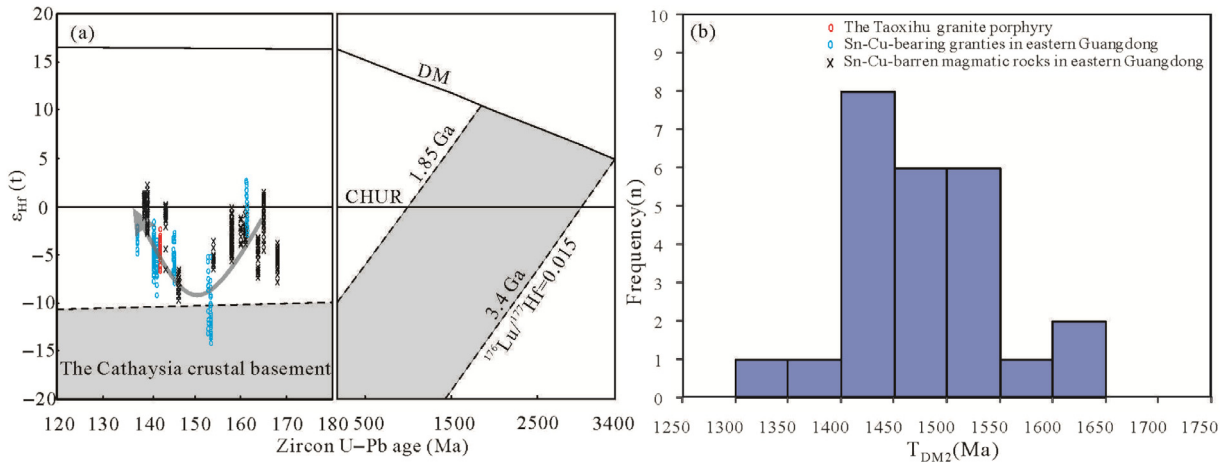

Fig. 9. (a) Diagram of zircon εHf(t) vs. U–Pb age for the Late Jurassic-Early Cretaceous volcanics and intrusions in eastern/SE Guangdong. The shaded field denotes the Cathaysia crustal basement (Xu et al., 2007; He and Xu, 2012). The Taoxihu granite porphyry data are from this study. Data sources for the other magmatic rocks are as in Table 9; (b) Histogram of T_{DM2} (Ma) for zircons from the Taoxihu granite porphyry.

2017a), Sanjiaowo that is intimately connected to the A type granite porphyry (cassiterite U–Pb: 139.8 ± 5.0 Ma; zircon U–Pb: 140.5 ± 1.4 Ma; Yan et al., unpublished data) and Taoxihu (this study). These Sn–W deposits are coeval with deposits in northern Jiangxi (e.g., Dahutang W: 139.2 ± 1.0 Ma; Mao et al., 2013b; Pengshan Sn deposits: 129.7 ± 2.5 Ma; Xu et al., 2015, 2016) and some deposits in Nanling area (e.g. Jubankeng W–Sn deposit: 139.2 ± 1.5 Ma; Fu et al., 2009; Bailashui Sn deposit: 137 ± 5 Ma; Li et al., 2006a; Dajishan W deposit: 144.0 ± 0.7 Ma; Zhang et al., 2006) suggest that a significant Sn–W mineralization event occurred between 145 and 130 Ma in southern China.

6.2. The Taoxihu granite porphyry: a fractionated I-type affinity

The Taoxihu granite porphyry contain lower (Zr + Nb + Ce + Y) concentrations (223–257 ppm) and zircon saturation temperatures (763–773 °C) than typical A-type granites (Zr + Nb + Ce + Y ≥ 350 ppm; Whalen et al., 1987; zircon saturation temperatures >800 °C; King et al., 1997). Whereas the rocks are high in $(K_2O + Na_2O)/CaO$ ratios, falling into the fractionated granite field in the $(K_2O + N_2O)/CaO$ vs. (Zr + Nb + Ce + Y) diagram (Fig. 14a), indicating its highly differentiated signature. Although no hornblende was identified, most of the samples have A/CNK values of

Table 5
Results of Re–Os dating of molybdenite from the Taoxihu deposit.

Spot no	Age (Ma)	$^{176}Yb/^{177}Hf$	$^{176}Lu/^{177}Hf$	$^{176}Hf/^{177}Hf$	1σ	ε_{Hf} (0)	ε_{Hf} (t)	1σ	t_{DM1} (Ma)	t_{DM2} (Ma)	$f_{Lu/Hf}$
Sample TXH-1: Granite porphy (excluding spot TXH-1-3, TXH-1-4, TXH-1-6, TXH-1-10, TXH-1-17)											
TXH-1-1	141.2	0.04033	0.00125	0.282603	0.000008	−5.99	-3.00	0.28	925	1386	−0.96
TXH-1-2	141.7	0.03098	0.00100	0.282531	0.000009	−8.52	−5.51	0.31	1020	1546	−0.97
TXH-1-5	141.6	0.03766	0.00118	0.282578	0.000008	−6.85	−3.85	0.29	958	1440	−0.96
TXH-1-7	145.9	0.04427	0.00136	0.282581	0.000009	−6.76	−3.69	0.32	959	1433	−0.96
TXH-1-8	142.8	0.02952	0.00093	0.282548	0.000008	−7.91	−4.86	0.30	994	1505	−0.97
TXH-1-9	142.7	0.03016	0.00096	0.282537	0.00001	−8.29	−5.25	0.35	1010	1530	−0.97
TXH-1-11	143.1	0.01903	0.00060	0.282588	0.000007	−6.52	−3.44	0.26	930	1415	−0.98
TXH-1-12	141.9	0.02508	0.00079	0.28255	0.000009	−7.84	−4.8.0	0.33	987	1501	−0.98
TXH-1-13	141.9	0.02907	0.00090	0.282587	0.000009	−6.55	−3.52	0.33	939	1419	−0.97
TXH-1-14	136.5	0.02127	0.00070	0.282501	0.000009	−9.6	−6.67	0.30	1054	1615	−0.98
TXH-1-15	142.6	0.02638	0.00082	0.282572	0.000009	−7.09	−4.04	0.31	958	1453	−0.98
TXH-1-16	141.6	0.02824	0.00087	0.282592	0.000007	−6.37	−3.34	0.26	931	1408	−0.97
TXH-1-18	141.8	0.0206	0.00066	0.282594	0.000008	−6.28	−3.23	0.28	922	1401	−0.98
TXH-1-19	142.2	0.01673	0.00055	0.28262	0.000009	−5.39	−2.32	0.33	885	1343	−0.98
TXH-1-20	140.9	0.04452	0.00138	0.282543	0.000009	−8.10	−5.14	0.33	1013	1521	−0.96
TXH-1-21	141.4	0.02268	0.00075	0.282558	0.000009	−7.56	−4.53	0.30	975	1483	−0.98
TXH-1-22	141.9	0.01659	0.00053	0.282566	0.000008	−7.29	−4.23	0.29	959	1464	−0.98
TXH-1-23	142.2	0.03411	0.00105	0.282557	0.000009	−7.60	−4.58	0.33	985	1487	−0.97
TXH-1-24	140.9	0.02302	0.00074	0.282514	0.000009	−9.11	−6.09	0.33	1036	1582	−0.98
TXH-1-25	142.8	0.02178	0.00068	0.282549	0.000009	−7.89	−4.82	0.32	986	1503	−0.98
TXH-1-26	141.5	0.02698	0.00087	0.282561	0.000009	−7.45	−4.42	0.33	974	1476	−0.97
TXH-1-27	141.8	0.02664	0.00083	0.282594	0.000008	−6.31	−3.27	0.29	928	1404	−0.97
TXH-1-28	141.7	0.03399	0.00118	0.282504	0.000013	−9.49	−6.49	0.47	1063	1608	−0.96
TXH-1-29	143.3	0.04175	0.00134	0.282574	0.000008	−6.99	−3.98	0.29	968	1449	−0.96
TXH-1-30	142.3	0.04257	0.00134	0.282561	0.000009	−7.48	−4.48	0.31	987	1480	−0.96

$\varepsilon Hf(t) = 10{,}000 \times (\{[(^{176}Hf/^{177}Hf)_S - (^{176}Lu/^{177}Hf)_S \times (e^{\lambda t} - 1)]/[(^{176}Hf/^{177}Hf)_{CHUR,\ 0} - (^{176}Lu/^{177}Hf)_{CHUR} \times ((e^{\lambda t} - 1)] - 1\}$. $T_{DM1} = 1/\lambda \times \ln\{1 + [(^{176}Hf/^{177}Hf)S - (^{176}Hf/^{177}Hf)_{DM}]/[(=Hf/^{177}Hf)_S - (^{176}Hf/^{177}Hf)_{DM}]\}$. $T_{DM2} = T_{DM1} - (T_{DM1} - t) \times [(fcc - fs)/(fcc - f_{DM})]$. $f_{Lu/Hf} = (^{176}Lu/^{177}Hf)_S/(^{176}Lu/^{177}Hf)_{CHUR} - 1$, where, $\lambda = 1.867 \times 10^{-11}/a$ (Söderlund et al., 2004); $(^{176}Lu/^{177}Hf)_S$ and $(^{176}Hf/^{177}Hf)_S$ are the measured values of the samples; $(^{176}Lu/^{177}Hf)_{CHUR} = 0.0332$ and $(^{176}Hf/^{177}Hf)_{CHUR,0} = 0.282772$ (Blichert-Toft and Albarede, 1997); $(^{176}Lu/^{177}Hf)_{DM} = 0.0384$ and $(^{176}Hf/^{177}Hf)_{DM} = 0.28325$ (Griffin et al., 2000); $(^{176}Lu/^{177}Hf)_{mean\ crust} = 0.015$; $fcc = [(^{176}Lu/^{177}Hf)mean\ crust/(^{176}Lu/^{177}Hf)_{CHUR}] - 1$; $fs = f_{Lu/Hf}$; $f_{DM} = [(^{176}Lu/^{177}Hf)_{DM}/(^{176}Lu/^{177}Hf)_{CHUR}] - 1$; t = crystallization time of zircon.

<1.1, which are indicative of I-type (Chappell and White, 1974, 1992). In addition, the granite porphyry contains much lower P_2O_5 (≤0.01 wt%) than typical S-type granites (>0.20%; Chappell, 1999) and a negative correlation with SiO_2, which also demonstrate its I-type affinity (Fig. 14b) (Chappell, 1999; Wu et al., 2003; Li et al., 2007b).

6.3. Magma source of the Taoxihu granitoids

Generally, petrogenetic models for the highly fractionated I-type magmas involve either extensive mafic magma fractionation (Chappell, 1999; Wyborn et al., 2001) or partial melting of crust materials (Chappell, 1999; Chappell et al., 2012). At Taoxihu, the granite porphyry has distinct Sr–Nd isotopic compositions from coeval mantle-derived mafic rocks in the region (Fig. 10b), which rules out the former possibility. This conclusion is also supported by the fact that the granite porphyry has relatively low Nb/Ta (8.60–9.35, mean = 9.02), and Th/U values (3.81–4.66, mean = 4.33), resembling those of the average crustal composition (Nb/Ta = 11, and Th/U = 4; Taylor and McLennan, 1985), suggesting a crustal source for the magma.

Therefore, we suggest that partial melting of crustal materials was the most plausible mechanism to generate the Taoxihu granite porphyry. The Taoxihu granite porphyry contains Mesoproterozoic T_{DM2} ages for both Nd and Hf isotopes, suggesting it was likely generated by partial melting of a crustal source of Mesoproterozoic overall residence age. Moreover, similar with coeval granites and volcanic rocks in eastern Guangdong, Hf isotope data of the Taoxihu granites plot slightly beneath the chondrite line and upon the domain of Cathaysia crustal basement rocks (Fig. 9a), suggesting possible mantle input in the partial melting process in this region (Fig. 9a; Zhao et al., 2012; Guo et al., 2012; Zhang et al., 2015; Qiu et al., 2017a,b; Liu et al., 2015). As shown in the $(^{87}Sr/^{86}Sr)_I$ vs. $\varepsilon_{Nd}(t)$ diagram, the Taoxihu data points are also plotted within the field of Late Jurassic-Early Cretaceous granitoids in central/eastern Guangdong, which were also interpreted as partial melting products of the ancient crust with varying degree of mantle-derived magma input (Fig. 10b; Ling et al., 2006; Zhang et al., 2015; Qiu et al., 2017b).

6.4. Metallogenic implications

6.4.1. Sources of sulfur and metals

The absence of sulfates at the Taoxihu deposit implies that the dominant sulfur species in the ore-forming fluids was H_2S instead of SO_4^{2-}, indicating that the sulfur isotope compositions ($\delta^{34}S$) of the sulfides approximate those of the bulk sulfur in the ore-forming fluids, i.e., $\delta^{34}S_{\sum S} \approx \delta^{34}S_{sulfide}$ (Hoefs, 2009; Ohmoto and Rye, 1979). The $\delta^{34}S_{CDT}$ values of the Taoxihu sulfides fall in a relatively narrow range (0.1–2.1‰), suggesting a dominantly magmatic sulfur origin (Ohmoto and Rye, 1979; Simon and Ripley, 2011). This is consistent with similar conclusions reached from many other magmatic-hydrothermal deposits in eastern Guangdong (Fig. 12b), such as the Sanjiaowo and Jinkeng Sn polymetallic deposits (Qiu et al., 2017a; Yan et al., unpublished data), Guantian Cu–Pb–Zn deposit (Xia, 2009), Lianhuashan W deposit (Zhang, 1985), Houpoao and Xiling Sn polymetallic deposits, and the Zhongqiuyang Cu polymetallic deposit (Lei, 1994; Xu, 1993).

As useful tracers of the sources of ore metals, the Pb isotopes provide important information about the nature of metal reservoir(s) and the geotectonic environment of mineralization. At Taoxihu, the sulfide Pb isotopes also show a relatively narrow range, suggesting a largely homogeneous lead source. The Taoxihu sulfide data span across the orogenic line and the upper crustal line (Fig. 11a), and fall closer to the orogenic line (Fig. 11b). This suggests that the primary lead source may have been the crust with

Table 6
Sr and Nd isotopic compositions of the Taoxihu granite.

Samples	Rb	Sr	$^{87}Rb/^{86}Sr$	$^{87}Sr/^{86}Sr_i$	2 σ Err.	$(^{87}Sr/^{86}Sr)_i$	Sm	Nd	$^{147}Sm/^{144}Nd$	$^{143}Nd/^{144}Nd$	2 σ Err.	εNd (0)	εNd (T)	$T_{DM,2}$(Ma)
TXH-1	346.5	57.7	17.5	0.7428318	0.000009	0.707660	8.1	32.9	0.148	0.512328	0.000005	−6.04	−5.17	1349
TXH-2	344.8	55.8	18.0	0.743926	0.000009	0.707730	8.5	36.1	0.142	0.512348	0.000005	−5.65	−4.67	1310
TXH-4	336.4	54.7	17.8	0.7433414	0.000010	0.707371	9.1	37.8	0.146	0.512327	0.000004	−6.07	−5.15	1348

Table 7
Lead isotopic compositions of whole rock (granite porphyry) and sulfides in the Taoxihu Sn deposit.

Sample No.	Mineral	$^{206}Pb/^{204}Pb$	$^{207}Pb/^{204}Pb$	$^{208}Pb/^{204}Pb$
TXH01	Pyrite	18.669	15.668	38.934
TXH02	Pyrite	18.665	15.673	38.899
TXH03	Pyrite	18.514	15.642	38.769
TXH04	Pyrite	18.497	15.646	38.764
TXH01	Chalcopyrite	18.536	15.667	38.776
TXH02	Chalcopyrite	18.557	15.659	38.812
TXH-1	Whole rock	18.682	15.656	38.944
TXH-2	Whole rock	18.657	15.654	38.922
TXH-3	Whole rock	18.674	15.652	38.937

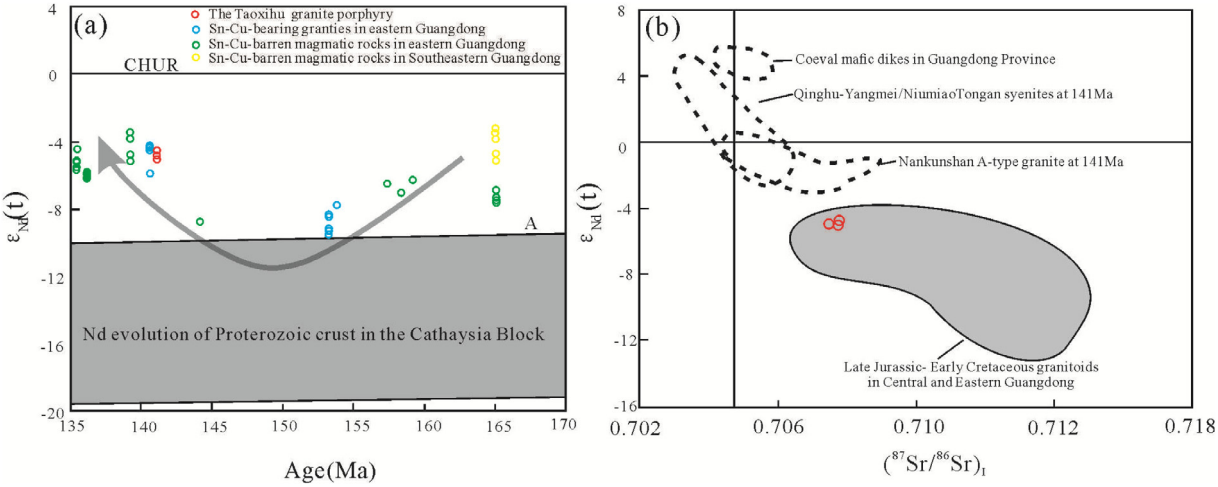

Fig. 10. Diagrams of (a) age vs. εNd(t) and (b) εNd(t) vs. $(87Sr/86Sr)_i$ for the Taoxihu granite porphyry and the Late Jurassic-Early Cretaceous volcanics and intrusions in eastern/SE Guangdong. Line A represents the Proterozoic crustal end-member of high degree of maturation in the Cathaysia Block, with average 147Sm/144Nd = 0.1132 and 143Nd/144Nd = 0.511568 (Shen et al., 2003); Line B represents the Proterozoic crustal end-member of low degree of maturation in the Cathaysia Block, with average 147Sm/144Nd = 0.1087 and 143Nd/144Nd = 0.512052 (Hu and Zhang, 1998). Data source: The Taoxihu granite porphyry (this study); Coeval mafic dikes (Li and McCulloch, 1998); The Qinghu-Yangmei/Niumiao-Tongan syenite (Li et al., 2004); The Nankunshan A-type granite (Li et al., 2007b); Late Jurassic-Early Cretaceous granitoids in central/eastern Guangdong (Ling et al., 2006; Xu and Yue, 1999b; Li et al., 2007b; Qiu et al., 2017b; Zhang et al., 2015). Data sources for the other magmatic rocks are as in Table 9.

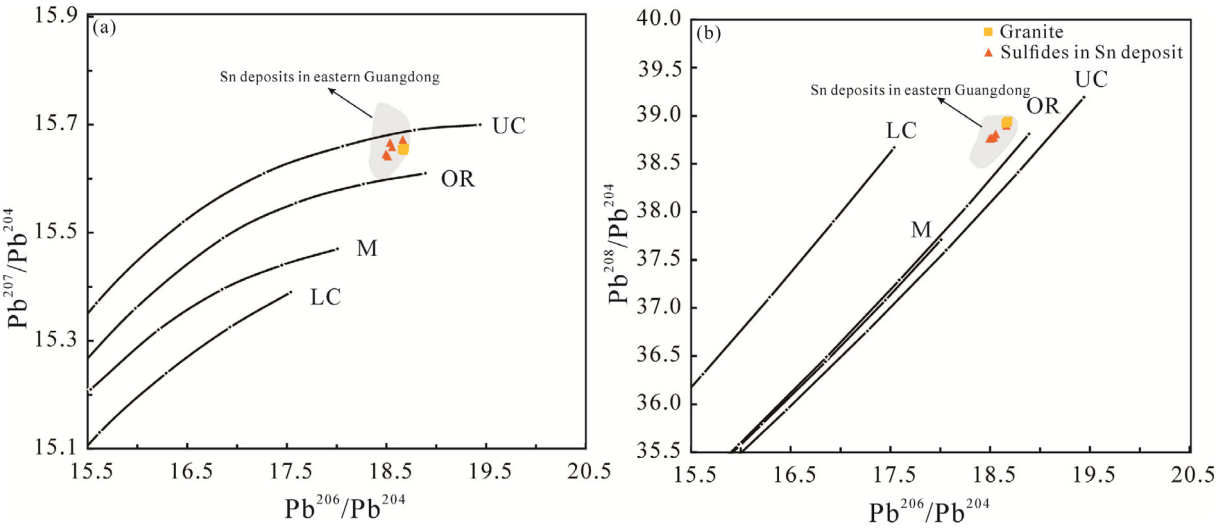

Fig. 11. Sulfide $\delta^{34}S$ histograms for (a) the Taoxihu Sn polymetallic deposit. (b) Major ore deposits in eastern Guangdong. Data of the Sanjiaowo, Taoxihu and Jinkeng deposits are from this study and the author's unpublished data, respectively. Other data are from Qiu et al. (2017b), Lei (1994), Xia (2009), Xu (1993) and Zhang (1985).

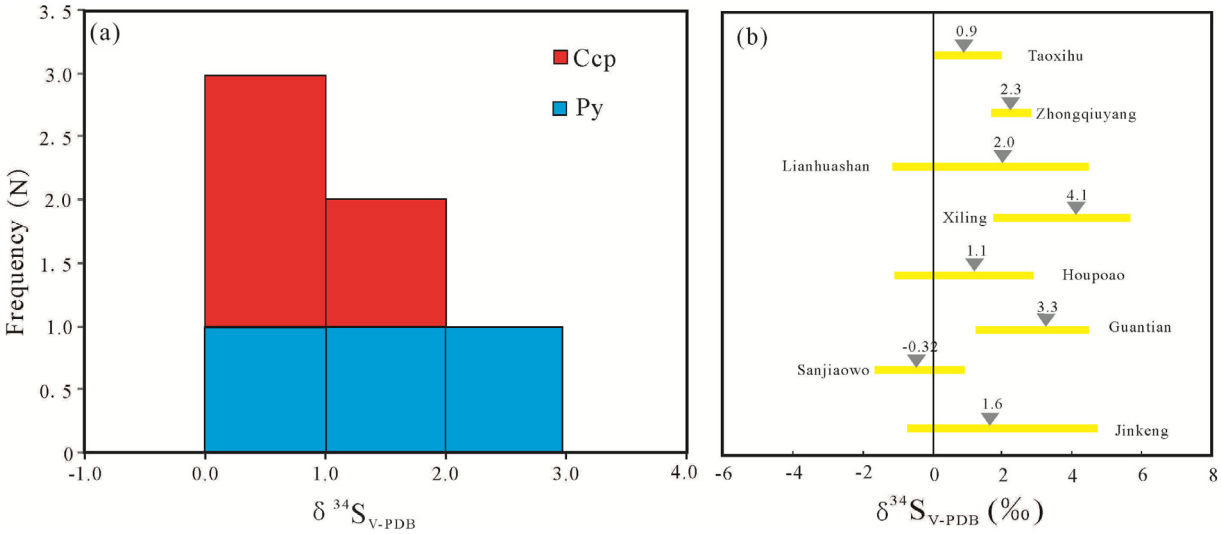

Fig. 12. Sulfide Pb isotope diagrams for the Taoxihu Sn deposit. Data are from the author's unpublished data. The base diagrams are from Zartman and Doe (1981). Abbreviations: UC = upper crust; OR = orogenic belt; M = mantle; LC = lower crust.

Table 8
Sulfur isotopic compositions of sulfides in the Taoxihu Sn deposit.

Sample No.	Occurance	Mineral	$\Delta^{34}S_{V\text{-}CDT}$ (‰)
TXH01	Veined- cassiterite-sulfides	Pyrite	0.7
TXH01	Veined- cassiterite-sulfides	Chalcopyrite	2.1
TXH02	Veined- cassiterite-sulfides	Pyrite	0.6
TXH02	Veined- cassiterite-sulfides	Chalcopyrite	0.1
TXH03	Quartz vein	Pyrite	1
TXH03	Quartz vein	Chalcopyrite	1

minor contribution from the mantle. Besides, in the Pb–Pb isotope diagram (Fig. 11), the data for Pb isotope in granite porphyry and in the sulfides of Taoxihu deposit plot in a broadly similar field, which may indicates a genetic connection between them.

Mao et al. (1999) firstly proposed that molybdenite Re concentrations increase from crustal to mantle source, a notion now widely accepted (e.g., Selby and Creaser, 2001; Stein et al., 2001; Berzina et al., 2005; Feng et al., 2011; Wu et al., 2015). At Taoxihu, the low molybdenite Re concentrations (52.3–231.1 ppb; average: 161.6 ppb) probably indicate significant crustal component, and are consistent with those of other crustal-sourced Sn polymetallic deposits in the region, such as Jinkeng (109.3–3257.6 ppb), Dadaoshan (155.2–193.0 ppb) and Feie'shan (43–1604 ppb) (Liu et al., 2015b).

6.4.2. Tin mineralization at Taoxihu

Fractional crystallization plays a very important role in concentrating incompatible elements, such as Sn, in the residual melt (Lehmann and Harmanto, 1990; Xu et al., 2016). Therefore, the highly fractionated nature of the Taoxihu granite would have facilitated the Sn mineralization. Oxygen fugacity (fO_2) of the magma, which controlled the degree of Sn enrichment, is another important metallogenic factor. Linnen et al. (1995) showed that under reducing conditions, tin is likely to exist as Sn^{2+} and enters the residual fluids, whereas under oxidizing conditions, Sn^{4+} ions tend to enter the early crystallizing minerals (Linnen et al., 1996). Both the calculated zircon Ce^{4+}/Ce^{3+} (10.2–108.2) and Eu_N/Eu_N^* (0.03–0.26) values of the Taoxihu granite indicate low fO_2 for the magma (Table 3), which would have facilitated Sn enrichment in the late hydrothermal fluids and thus the Sn mineralization.

The substantially higher Sn (13–31 ppm, average: 21 ppm; Table 1) than the average upper and lower crust (5.5 ppm and 1.5 ppm, respectively; Taylor and McLennan, 1985), as well as the elevated F (1710–3780 ppm, average: 3020 ppm; Table 1) of the Taoxihu granite porphyry indicate that it is a typical F-specialized Sn-bearing granite (Lehmann and Harmanto, 1990). This, together with the deposit geology, age, geochemical and isotope evidence abovementioned, suggest that the ore-forming fluids were likely derived from the granite porphyry.

6.5. Tectonic implications

It is generally accepted that South China (especially the SE coastal region) was tectonically influenced by the Paleo-Pacific tectonics since the Middle Jurassic (Zhou et al., 2006; Li et al., 2006b; Liu et al., 2012; Wang et al., 2003; Zhang et al., 2012). Regional extension was suggested to have occurred during ca. 165–150 Ma, as evidenced by the coeval alkaline and bimodal magmatism and A-type granites (e.g., Jiang et al., 2009; Li et al., 2007b; Zhu et al., 2010). In recent years, extensive Jurassic igneous activity (dominantly granitic) has been documented in the coastal area of Guangdong, which is interpreted to have formed in an extensional setting (Huang et al., 2013; Zhang et al., 2013; Qiu et al., 2017b).

A regional compressive event was proposed to have occurred during the Jurassic-Cretaceous boundary, as evidenced by the magmatic quiescence and regional unconformity in most of the South China Block has been documented by many researches (e.g., Zhang et al., 2013; Yang et al., 2012; Li et al., 2014; Hu and Zhou, 2012; Wong et al., 2009; Zhou et al., 2016). The compressive tectonics also identified in the eastern Guangdong. Fig. 15 shows that magmatic-metallogenic quiescence was likely to occur during ca. 152–147 Ma in eastern Guangdong. This is in agreement with the slightly decreasing zircon εHf(t) and bulk rock εNd(t) values from 165 to 153 Ma (indicating less juvenile mantle input), and increas-

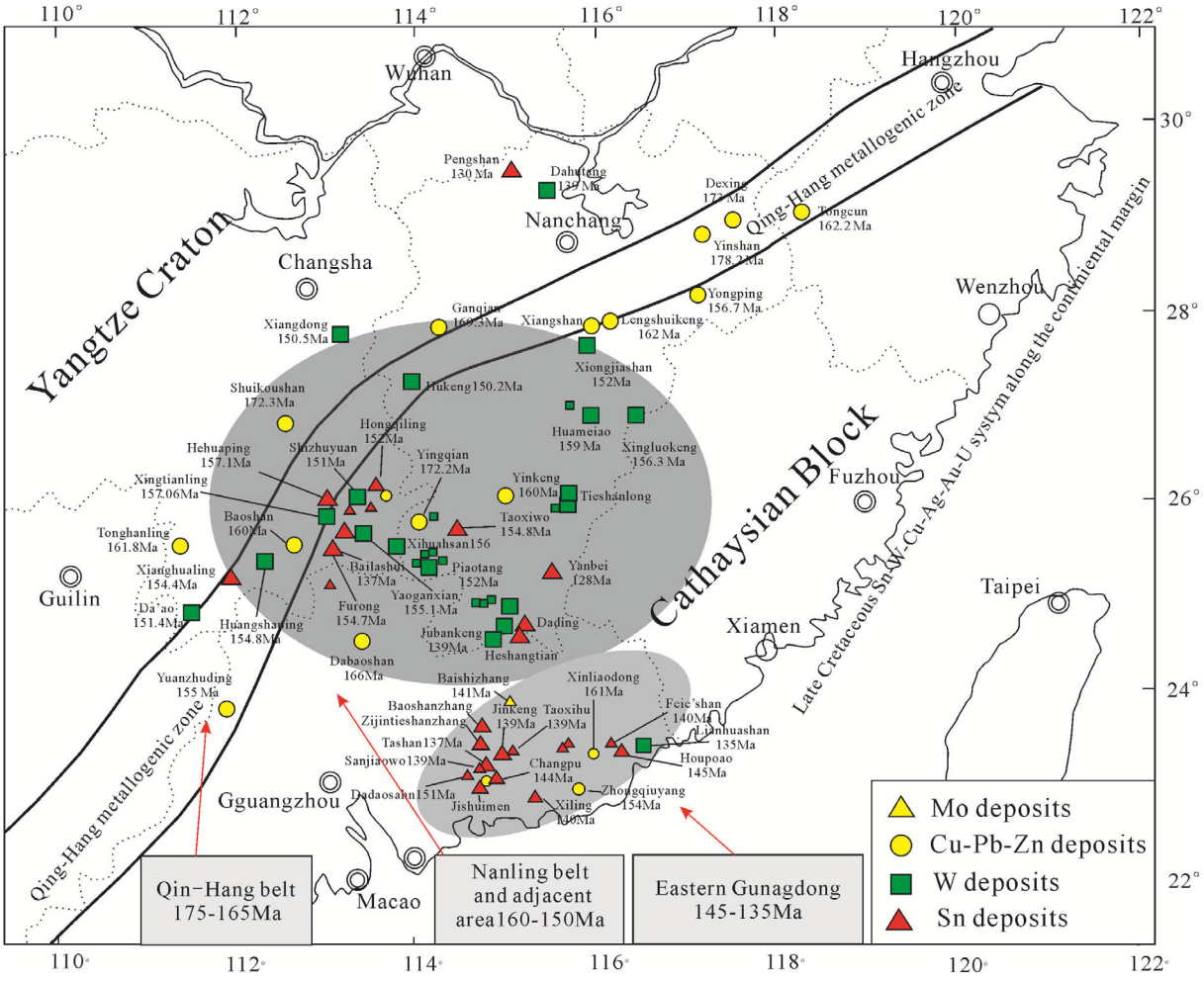

Fig. 13. Diagrams of (a) $(K_2O + Na_2O)/CaO$ vs. (Zr + Nb + Ce + Y) (Whalen et al., 1987); (b) SiO_2 vs. P_2O_5 for the Taoxihu granite porphyry. The I- and S-type granite compositional trends are from Wu et al. (2003) and Li et al. (2007b).

Table 9
Compilation of igneous rocks and Sn–W mineralization ages, Hf and Nd isotopic compositions of magmatic rocks in Eastern and Southeastern Guangdong.

Deposit/pluton	Lithology	Measured objects	Method	Age (Ma)	εHf (t)	T_{DM2} (Ma)	εNd (t)	T_{DM2} (Ma)	Reference
Eastern Guangdong									
Dadaoshan Sn deposit	Porphyritic granite	Zircon	LA–ICPMS U–Pb	153.2 ± 1.2	−14.2 to −5.1	1.64–1.81	−9.48 to −8.54	1.64–1.81	Qiu et al. (2017b)
		Molybdenite	Re–Os isochron	152.8 ± 7.8					
Jinkeng Sn polymetallic deposit	Biotite granite	Zircon	LA–ICPMS U–Pb	144.7 ± 0.8	−7.6 to −3.2	1.41–1.68			Qiu et al. (2017a)
	Fine-grained granite	Zircon	LA–ICPMS U–Pb	141.1 ± 1.3	−9.2 to −3.5	1.42–1.78			
		Molybdenite	Re–Os isochron	139.3 ± 2.5					
Sanjiaowo Sn deposit	Granite porphyry	Zircon	LA–ICPMS U–Pb	140.5 ± 1.4	−8.4 to −4.2	1.46–1.72	−5.9 to −4.0	1.26–1.41	Authors' unpublished data
		Cassiterite	LA–ICPMS U–Pb	139.8 ± 5.0					
Taoxihu Sn polymetallic deposit	Granite porphyry	Zircon	LA–ICPMS U–Pb	141.8 ± 1.0	−6.7 to −2.3	1.34–1.62	−5.17 to −4.67	1.31–1.35	This study
		Molybdenite	Re–Os isochron	139.0 ± 0.8					
Tashan Sn polymetallic deposit	Granite porphyry	Zircon	LA–ICPMS U–Pb	136.8 ± 1.1	−4.9 to −2.1	1.32–1.51			Authors' unpublished data
		Cassiterite	LA–ICPMS U–Pb	136.5 ± 8.1					
Changpu Sn polymetallic deposit	Quartz porphyry	Zircon	LA–ICPMS U–Pb	145.0 ± 0.9	−8.0 to −2.7	1.37–1.70			Qiu et al. (2016)
Tiandong W–Sn deposit	Medium-grained granite	Zircon	LA–ICPMS U–Pb	191.5 ± 0.9	+4.0 to +9.8	0.61–0.98			Liu et al. (2015b)

(*continued on next page*)

Table 9 (*continued*)

Deposit/pluton	Lithology	Measured objects	Method	Age (Ma)	εHf (t)	T_{DM2} (Ma)	εNd (t)	T_{DM2} (Ma)	Reference
	Coarse-grained granite	Zircon	LA–ICPMS U–Pb	158.0 ± 1.3	−3.6 to −0.1	1.22–1.44			
	Fine-grained biotite granite	Zircon	LA–ICPMS U–Pb	140.5 ± 0.8	−5.4 to −1.6	1.33–1.42			
Feie'shan W-Sn deposit	Granite porphyry	Zircon	LA–ICP–MS	139.2 ± 1.7					Liu et al. (2017)
		Molybdenite	Re–Os weighted average of model age	140.6 ± 1.9					
		Biotite	Ar–Ar	135.1 ± 10.8					
Xinliaodong Cu deposit	Quartz diorite	Zircon	LA–ICP–MS	161 ± 1	−2.8 to +2.7	1.03–1.58			Wang et al. (2016)
	Biotite granite	Zircon	SHRIMP	162.3 ± 1.4					Authors' unpublished data
	Granodiorite	Zircon	SHRIMP	160.2 ± 1.4					Authors' unpublished data
Anliu	Monzogranite	Zircon	LA–ICP–MS	145.6	−10.1 to −6.8	1.63–1.83			Authors' unpublished data
Yuanpanbei	Biotite granite	Zircon	LA–ICP–MS	152.8 ± 4.5	−13.7 to −5.1	1.52–2.07			Authors' unpublished data
Hopoao Sn polymetallic deposit	Monzogranite	Whole rock	Rb–Sr ischron	144.9 ± 9.4					Xu and Yue (1999)
		Sericite	Ar–Ar isochron	145.4 ± 1.9					
Lianhuashan W deposit	Biotite granite	Whole rock	Rb–Sr ischron	137.2 ± 2.5					Ni et al. (1983)
		Muscovite	Rb–Sr isochron	135					
Mantoushan	Syeno-monzogranites and alkali feldspar granites	Zircon	LA–ICPMS U–Pb	166–161	−7.4 to −3.2	1.26–1.48	−7.8 to −6.9	1.51–1.59	Zhou et al. (2016)
Hulutian	Alkali feldspar granites	Zircon	LA–ICPMS U–Pb	139 ± 2	−0.7 to +1.8	0.96–1.10	−5 to −3.4	0.96–1.10	
Longwo	Granodiorite	Zircon	LA–ICPMS U–Pb	165.2 ± 1.9	−4.6 to −0.9	1.27–2.17			Zhang et al. (2015)
Lianhuashan	Granodiorite	Zircon	SIMS U–Pb	154.3 ± 1.4	−6.5 to −3.6	1.43–1.61	−7.6	1.6	
Wushikeng	Biotite granite	Zircon	LA–ICPMS U–Pb	159.7 ± 1.7	−4.0 to +3.9	0.96–1.47	−6.2	1.5	
Shigushan	Biotite granite	Zircon	SIMS U–Pb	158.5 ± 1.3	−5.1 to −2.5	1.37–1.54	−7	1.5	
Chiliao	Biotite granite	Zircon	LA–ICPMS U–Pb	157.2 ± 1.8	−5.6 to −3.2	1.41–1.57	−6.5	1.5	
Fenghuang	Biotite granite	Zircon	LA–ICPMS U–Pb	161.3 ± 1.2	−3.9 to −0.3	1.23–1.46			
Dabu	Biotite granite	Zircon	LA–ICPMS U–Pb	136.3 ± 0.6					Zhao et al. (2012)
Jiexi	Biotite-K-spar granite	Zircon	LA–ICPMS U–Pb	134.9 ± 0.4					
Nianshan	Medium-grained biotite granite	Zircon	LA–ICPMS U–Pb	144			−8.7	1.6	Ling et al. (2006)
Douling Formation in Fengshun basin	Dacite	Zircon	LA–ICPMS U–Pb	168.2 ± 2.0	−7.8 to −3.8	1.46–1.71			Guo et al. (2012)
	Rhyolite	Zircon	LA–ICPMS U–Pb	142.7 ± 1.0	−6.5 to +0.3	1.24–1.62			
	Dacite	Zircon	LA–ICPMS U–Pb	165.0 ± 1.0	−3.9 to +1.5	1.22–1.48			
	Rhyolite	Zircon	LA–ICPMS U–Pb	145.8 ± 2.0					
	Dacite	Zircon	LA–ICPMS U–Pb	143.3 ± 0.5					
	Dacite	Zircon	SIMS U–Pb	139.0 ± 1.0	−2.8 to +2.3	1.23–1.37			
Sanjiaowo	Mafic dikes	Zircon	SIMS U–Pb	140.3 ± 2.5					Authors' unpublished data
Tangwei	Mafic dikes	Zircon	SIMS U–Pb	143.2 ± 2.3					
Anliu	Mafic dikes	Zircon	SIMS U–Pb	152.9 ± 3.0					
Jishuimen	Mafic dikes	Zircon	SIMS U–Pb	141.7 ± 3.2					
GD16(2)	Mafic dikes	Whole rock	K-Ar	146.48 ± 3.13					Cao et al. (2009)
GD20(1)	Mafic dikes	Whole rock	K-Ar	132.41 ± 3.28					
Southeastern Guangdong									
Guangwei		Zircon	SIMS U–Pb	165.7 ± 1.3	−2.2 to −0.2	1.22–1.35	−6.46 to −3.13	1.47–1.20	Huang et al. (2013)
Xiaoliang		Zircon	SIMS U–Pb	159.4 ± 1.3	−5.9 to	1.29–1.59			

Table 9 (*continued*)

Deposit/pluton	Lithology	Measured objects	Method	Age (Ma)	εHf (t)	T_{DM2} (Ma)	εNd (t)	T_{DM2} (Ma)	Reference
Guduoshan		Zircon	SIMS U–Pb	160.7 ± 1.3	−1.2 to −9.9 to −5.9	1.58–1.84			
Wuguishan		Zircon	SIMS U–Pb	159.5 ± 1.6	−11.4 to −7.0	1.65–1.93			

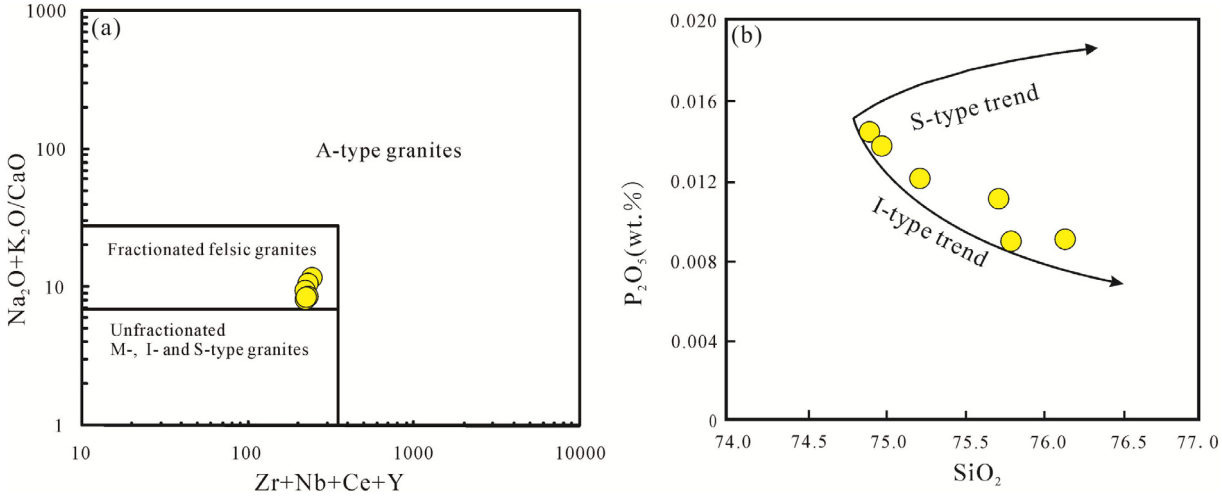

Fig. 14. Distribution of major Mesozoic ore deposits in South China (modified after Mao et al., 2013; Chen et al., 2014).

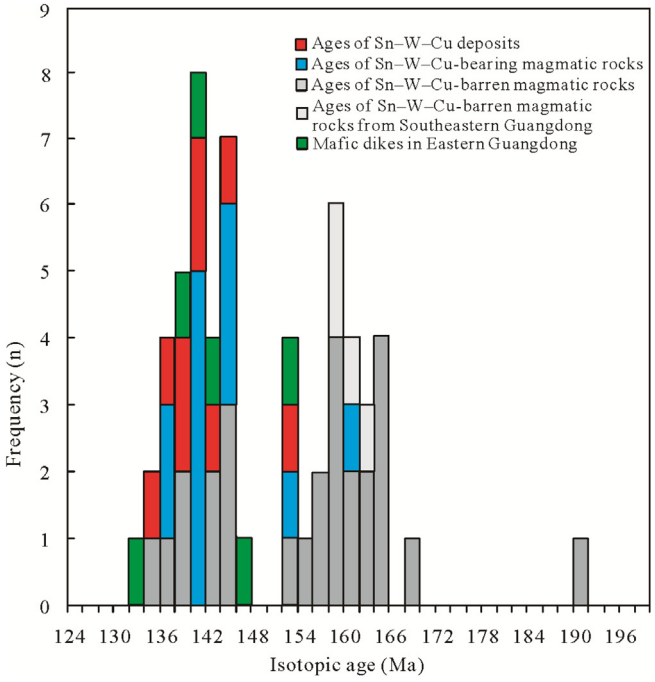

Fig. 15. Age histogram for the Sn–W deposits, Sn–W-bearing/barren igneous rocks and mafic dikes in eastern/SE Guangdong. Data sources are as in Table 9.

ing values from 146 to 135 Ma (indicating more juvenile mantle input) (Figs. 9 and 10). Therefore, we propose that the regional compression may have occurred during ca. 152–147 Ma.

In the Early Cretaceous, the widespread alkaline/bimodal magmatism and A-type granite (including Sanjiaowo A-type granite in eastern Guangdong: ca. 141 Ma; Yan et al., unpublished data) events, as well as the basin-and-range tectonics all suggest a dominantly extensional tectonic regime in South China (Yang et al., 2012; Li et al., 2014; Shu et al., 2009; Zhou et al., 2016; Yan et al., unpublished data). This period of extension was generally considered to be related to the subduction slab roll-back of the Paleo-Pacific Plate from around 145 Ma (e.g., Liu et al., 2015) which is consistent with the second peak of magmatism during 146–135 Ma after short compression during Jurassic-Cretaceous boundary in eastern Guangdong. The resultant lithospheric extension may have induced asthenospheric upwelling, which triggered the partial melting of the metamorphic basement rocks of Mesoproterozoic overall residence age and generated the Sn-bearing granitic magma in eastern Guangdong.

7. Conclusions

(1) The Early Cretaceous Taoxihu Sn polymetallic mineralization (139 ± 1.1 Ma) was likely genetically linked to the granite porphyry (141.8 ± 1.0 Ma).
(2) Geochemical and Sr–Nd–Hf isotopic data indicate that the Taoxihu granite porphyry is highly a fractionated I-type, generated by partial melting of the Mesoproterozoic crust with minor mantle input. The crustal partial melting and Sn mineralization may have occurred during the mantle underplating in an extensional environment, probably associated with the subduction slab roll-back of the Paleo-Pacific Plate.

Acknowledgments

This research was financially supported by China Geological Survey Package Exploration Key Basic Geology Research Project (Grant No. 12120114015901). We thank the staff of Geology Bureau for Nonferrous Metals of Guangdong Province. State Key Laboratory of Isotope Geochemistry, Guangzhou Institute of Geochemistry, Chinese Academy of Sciences (GIGCAS), and CAS Key Laboratory of Mineralogy and Metallogeny, GIGCAS are acknowledged for LA–ICPMS zircon U–Pb dating, Hf isotope analyses, major and trace element analyses, and Re–Os dating.

References

Andersen, T., 2002. Correction of common lead in U-Pb analyses that do not report Pb. Chem. Geol. 192, 59–79.

Ballard, J., Palin, M., Campbell, I., 2002. Relative oxidation states of magmas inferred from Ce(IV)/Ce(III) in zircon: application to porphyry copper deposits of northern Chile. Contrib. Mineral. Petrol. 144, 347–364.

Belousova, E.A., Griffin, W.L., O'Reilly, S.Y., Fisher, N.I., 2002. Igneous zircon: trace element composition as an indicator of source rock type. Contrib. Miner. Petrol. 14 (5), 602–622.

Berzina, A.N., Sotnikov, V.I., Economou-Eliopoulos, M., Eliopoulos, D.G., 2005. Distribution of rhenium in molybdenite from porphyry Cu–Mo and Mo–Cu deposits of Russia (Siberia) and Mongolia. Ore Geol. Rev. 26, 91–113.

Black, L.P., Kamo, S.L., Allen, C.M., Aleinikoff, J.N., Davis, D.W., Korsch, R.J., Foudoulis, C., 2003. TEMORA 1: a new zircon standard for Phanerozoic U-Pb geochronology. Chem. Geol. 200 (1), 155–170.

Blichert-Toft, J., Albarede, F., 1997. The Lu–Hf isotope geochemistry of chondrites and the evolution of the mantle-crust system. Earth Planet. Sci. Lett. 148, 243–258.

Cao, J.J., Hu, R.Z., Xie, G.Q., Liu, S., 2009. Geochemistry and genesis of mafic dikes from the coastal areas of Guangdong Province, China. Acta Petrologica Sinica 25 (4), 984–1000.

Chappell, B.W., 1999. Aluminium saturation in I- and S-type granites and the characterization of fractionated haplogranites. Lithos 46, 535–551.

Chappell, B.W., White, A.J.R., 1974. Two contrasting granite types. Pac. Geol. 8, 173–174.

Chappell, B.W., White, A.J.R., 1992. I- and S-type granites in the Lachlan Fold Belt. GSA Special Papers 272, 1–26.

Chappell, B.W., Bryant, C.J., Wyborn, D., 2012. Peraluminous I-type granites. Lithos 153, 142–153.

Chen, Y.C., Wang, D.H., Xu, Z.G., Huang, F., 2014. Outline of regional metallogeny of ore deposits associated with the Mesozoic magmatism in South China. Geotectonica Metallogenia 38 (2), 219–229 (in Chinese with English abstract).

Feng, C.Y., Zeng, Z.L., Zhang, D.Q., Qu, W.J., Du, A.D., Li, D.X., She, H.Q., 2011. SHRIMP zircon U-Pb and molybdenite Re–Os isotopic dating of the tungsten deposits in the Tianmenshan-Hongtaoling W–Sn orefield, southern Jiangxi Province, China, and geological implications. Ore Geol. Rev. 43, 8–25.

Fu, J.M., Li, X.N., Cheng, S.B., Xu, D.M., Ma, L.Y., Chen, X.Q., 2009. Metallogenic ages of tungsten-tin polymetallic deposits in Lianping area, northern Guangdong Province. Geol. China 36, 1331–1339 (in Chinese with English abstract).

Giesemann, A., Jäger, H.J., Norman, A.L., Krouse, H.R., Brand, W.A., 1994. Online sulfur-isotope determination using an elemental analyzer coupled to a mass spectrometer. Anal. Chem. 66, 2816–2819.

Griffin, W.L., Pearson, N., Belousova, E., Jackson, S., Van Achterbergh, E., O'Reilly, S.Y., Shee, S., 2000. The Hf isotope composition of cratonic mantle: LA-MC-ICP-MS analysis of zircon megacrysts in kimberlites. Geochim. Cosmochim. Acta 64, 133–147.

Griffin, W.L., Wang, X., Jackson, S.E., Pearson, N.J., O'Reilly, S.Y., 2002. Zircon geochemistry and magma mixing, SE China: in-situ analysis of Hf isotopes, Tonglu and Pingtan igneous complexes. Lithos 61, 237–269.

Guangdong Nonferrous Metals Geological Bureau 931 Battalion (GNMGB), 2014. Reconnaissance report of the Taoxihu Sn polymetallic deposit in Jiexi County, Guangdong Province. Unpublished report, pp. 1–38. (in Chinese).

Guo, F., Fan, W.M., Li, C.W., Zhao, L., Li, H.X., Yang, J.H., 2012. Multi-stage crust–mantle interaction in SE China: temporal, thermal and compositional constraints from the Mesozoic felsic volcanic rocks in eastern Guangdong-Fujian provinces. Lithos 150, 62–84.

He, Z.Y., Xu, X.S., 2012. Petrogenesis of the Late Yanshanian mantle-derived intrusions in southeastern China: response to the geodynamics of paleo-Pacific plate subduction. Chem. Geol. 328, 208–221.

Hoefs, J., 2009. Stable Isotope Geochemistry. Springer Verlag, Berlin, Heidelberg, pp. 130–135.

Hoskin, P.W.O., Schaltegger, U., 2003. The composition of zircon and igneous and metamorphic petrogenesis. Rev. Mineral. Geochem. 53 (1), 27–62.

Hu, G.R., Zhang, B.D., 1998. Neodymium isotope compositions and source materials of the meta-basement in Central Jiangxi Province. Acta Petrol. Mineral. 17, 35, 35 Neodyinese with English abstract.

Hu, R.Z., Zhou, M.F., 2012. Multiple Mesozoic mineralization events in South China—an introduction to the thematic issue. Miner. Deposita 47, 579–588.

Hua, R.M., Chen, P.R., Zhang, W.L., Lu, J.J., 2005. Three major metallogenic events in Mesozoic in South China. Mineral Deposits 24 (2), 99–107 (in Chinese with English abstract).

Huang, L.C., Jiang, S.Y., 2014. Highly fractionated S-type granites from the giant Dahutang tungsten deposit in Jiangnan Orogen, Southeast China: geochronology, petrogenesis and their relationship with W-mineralization. Lithos 202, 207–226.

Huang, H.Q., Li, X.H., Li, Z.X., Li, W.X., 2013. Intraplate crustal remelting as the genesis of Jurassic high-K granites in the coastal region of the Guangdong Province, SE China. J. Asian Earth Sci. 74, 280–302.

Jiang, Y.H., Jiang, S.Y., Dai, B.Z., et al., 2009. Middle to late Jurassic felsic and mafic magmatism in Southern Hunan Province, Southeast China: implications for a continental arc to rifting. Lithos 107 (3), 185–204.

King, P.L., White, A., Chappell, B.W., Allen, C.M., 1997. Characterization and origin of aluminous A-type granites from the Lachlan Fold Belt, southeastern Australia. J. Petrol. 38, 371–391.

Lehmann, B., Harmanto, 1990. Large-scale tin depletion in the Tanjungpandan tin granite, Belitung Island, Indonesia. Econ. Geol. 85, 99–111.

Lei, X.Y., 1994. Stable isotope geochemical studies of the tin-polymetallic deposits in eastern Guangdong Province. Mineral Deposits 13, 322–330 (in Chinese with English abstract).

Li, X.H., McCulloch, M.T., 1998. Geochemical characteristics of Cretaceous mafic dikes from northern Guangdong, SE China: age, origin and tectonic significance. In: Mantle Dynamics and Plate Interactions in East Asia, pp. 405–419.

Li, X.H., Li, Z.X., Zhou, H.W., Liu, Y., Kinny, P.D., 2002. U-Pb zircon geochronology, geochemistry and Nd isotopic study of Neoproterozoic bimodal volcanic rocks in the Kangdian Rift of South China: implications for the initial rifting of Rodinia. Precambr. Res. 113, 135–154.

Li, X.H., Li, Z.X., Ge, W.C., Zhou, H.W., Li, W.X., Liu, Y., Wingate, M.T.D., 2003. Neoproterozoic granitoids in South China: crustal melting above a mantle plume at ca. 825 Ma? Precambr. Res. 122, 45–83.

Li, X.H., Chen, Z.G., Liu, D.Y., Li, W.X., 2003b. Jurassic gabbro-granite-syenite suites from southern Jiangxi Province (SE China): age, origin and tectonic significance. Int. Geol. Rev. 45, 898–921.

Li, X.H., Chuang, S.L., Zhou, X.W., Lo, C.H., Liu, Y., Chen, C.H., 2004. Jurassic intraplate magmatism in southern Hunan-eastern Guangxi: $^{40}Ar/^{39}Ar$ dating, geochemistry, Sr-Nd isotopes and implications for tectonic evolution of SE China. In: Malpas, J., Fletcher, C.J., Aitchison, J.C., Ali, J. (Eds.), Aspects of the Tectonic Evolution of China, vol. 226. Geological Society of London Special Publications, pp. 193–216.

Li, H.Q., Lu, Y.F., Wang, D.H., Chen, Y.C., Yang, H.M., Guo, J., Xie, C.F., Yang, Y.P., Ma, L. Y., 2006a. Dating of the rock-forming and ore-forming ages and their geological significances in the Furong ore-field, Qitian Mountain, Hunan. Geol. Rev. 51 (1), 113–121 (in Chinese with English abstract).

Li, X.H., Li, Z.X., Li, W.X., Wang, Y.J., 2006b. Initiation of the Indosinian orogeny in South China: evidence for a Permian magmatic arc on Hainan island. J. Geol. 114, 341–353.

Li, X.H., Li, Z.X., Li, W.X., Liu, Y., Yuan, C., Wei, G.J., Qi, C.S., 2007b. U-Pb zircon, geochemical and Sr–Nd–Hf isotopic constraints on age and origin of Jurassic I- and A-type granites from central Guangdong, SE China: a major igneous event in response to foundering of a subducted flat-slab? Lithos 96, 186–204.

Li, Z.L., Hu, R.Z., Yang, J.S., Peng, J.T., Li, X.M., Bi, X.W., 2007c. He, Pb and S isotopic constraints on the relationship between the A-type Qitianling granite and the Furong tin deposit, Hunan Province, China. Lithos 97 (1), 161–173.

Li, X.H., Long, W.W., Li, Q.L., Liu, Y., Zheng, Y.F., Yang, Y., Chamberlain, K.R., Wan, D., Guo, C., Wang, X., 2010. Penglai zircon megacrysts: a potential new working reference material for microbeam determination of Hf–O isotopes and U-Pb age. Geostand. Geoanal. Res. 34, 117–134.

Li, H., Zhang, H., Ling, M.X., Wang, F.Y., Ding, X., Zhou, J.B., Yang, X.Y., Tu, X.L., Sun, W.D., 2011. Geochemical and zircon U-Pb study of the Huangmeijian A-type granite: implications for geological evolution of the Lower Yangtze River belt. Int. Geol. Rev. 53, 499–525.

Li, Z., Qiu, J.S., Yang, X.M., 2014. A review of the geochronology and geochemistry of Late Yanshanian (Cretaceous) plutons along the Fujian coastal area of southeastern China: implications for magma evolution related to slab break-off and rollback in the Cretaceous. Earth Sci. Rev. 128, 232–248.

Liang, X.R., Wei, G.J., Li, X.H., Liu, Y., 2003. Precise measurement of $^{143}Nd/^{144}Nd$ and Sm/Nd ratios using multiple-collectors inductively coupled plasma-mass spectrometer (MCICPMS). Geochimica 32, 91–96.

Ling, H.F., Shen, W.Z., Sun, T., Jiang, S.Y., Jiang, Y.H., Ni, P., 2006. Genesis and source characteristics of 22 yanshanian granites in guangdong province: study of element and nd-sr isotopes. Acta Petrologica Sinica 22 (11), 2687–2703.

Linnen, R.L., Pichavant, M., Holtz, F., Burgess, S., 1995. The effect of $fO2$ on the solubility, diffusion, and speciation of tin in haplogranitic melt at 850 °C and 2 kbar. Geochim. Cosmochim. Acta 59 (8), 1579–1588.

Linnen, R.L., Pichavant, M., Holtz, F., 1996. The combined effects of fO_2 and melt composition on SnO_2 solubility and tin diffusivity in haplogranitic melts. Geochim. Cosmochim. Acta 60 (24), 4965–4976.

Liu, Y.S., Gao, S., Hu, Z.C., Gao, C.G., Zong, K.Q., Wang, D.B., 2010. Continental and oceanic crust recycling-induced melt–peridotite interactions in the Trans-North China Orogen: U-Pb dating, Hf isotopes and trace elements in zircons from mantle xenoliths. J. Petrol. 51, 537–571.

Liu, X., Fan, H.R., Santosh, M., Hu, F.F., Yang, K.F., Li, Q.L., Yang, Y.H., Liu, Y.S., 2012. Remelting of Neoproterozoic relict volcanic arcs in the Middle Jurassic: implication for the formation of the Dexing porphyry copper deposit, Southeastern China. Lithos 150, 85–100.

Liu, L., Xu, X., Xia, Y., 2015a. Asynchronizing paleo-Pacific slab rollback beneath SE China: insights from the episodic Late Mesozoic volcanism. Gondwana Res. http://dx.doi.org/10.1016/j.gr.2015.09.009.
Liu, P., Cheng, Y.B., Mao, J.W., Wang, X.Y., Yao, W., Cheng, X.T., Zeng, X.J., 2015b. Zircon U-Pb age and Hf isotopic characteristics of granite from the Tiandong W-Sn polymetallic deposit in Eastern Guangdong Province and its significance. Acta Geol. Sinica 89 (5), 1244–1257 (in Chinese with English abstract).
Liu, P., Mao, J., Cheng, Y., Yao, W., Wang, X., Hao, D., 2017. An Early Cretaceous W-Sn deposit and its implications in southeast coastal metallogenic belt: constraints from U-Pb, Re-Os, Ar-Ar geochronology at the Feie'shan W-Sn deposit, SE China. Ore Geol. Rev. 81, 112–122.
Ludwig, K.R., 2003. User's Manual for Isoplot/Ex Version 3.00—A Geochronology Toolkit for Microsoft Excel. Berkeley Geochronology Center Special Publication 4, 1–70.
Maniar, P.D., Piccoli, P.M., 1989. Tectonic discrimination of granitoids. Geol. Soc. Am. Bull. 101 (5), 635–643.
Mao, J.W., Zhang, Z.C., Zhang, Z.H., Du, A.D., 1999. Re–Os isotopic dating of molybdenites in the Xiaoliugou W–(Mo) deposit in the northern QilianMountains and its geological significance. Geochim. Cosmochim. Acta 63, 1818–1845.
Mao, J.W., Cheng, Y.B., Chen, M.H., Pirajno, F., 2013. Major types and time–space distribution of Mesozoic ore deposits in South China and their geodynamic settings. Miner. Deposita 48, 267–294.
Mao, Z.H., Cheng, Y.B., Liu, J.J., Yuan, S.D., Wu, S.H., Xiang, X.K., Luo, X.H., 2013b. Geology and molybdenite Re–Os age of the Dahutang granite-related veinlets-disseminated tungsten ore field in the Jiangxi Province, China. Ore Geol. Rev. 53, 422–433.
Ni, S.B., Man, F.S., Bai, Y.Z., Li, T., 1983. Rr–Sr dating of Lianhuashan tungsten ore deposit. J. China Univ. Sci. Technol. 13, 246–252 (in Chinese with English abstract).
Ohmoto, H., Rye, R.O., 1979. Isotopes of sulfur and carbon. In: Barnes, H.L. (Ed.), Geochemistry of Hydrothermal Ore Deposits. ed. 2. John Wiley and Sons, New York, pp. 509–567.
Peccerillo, A., Taylor, S.R., 1976. Geochemistry of Eocene calc-alkaline volcanic rocks from the Kastamonu area, northern Turkey. Contrib. Miner. Petrol. 58, 63–81.
Qiu, Y.X., Qiu, J.S., Li, J.C., Zhong, H.P., 1991. Deformational and metamorphic features of Lianhuashan fault zone during Mesozoic time and mechanism of their formation. J. Geomech. 14, 93–106 (in Chinese with English abstract).
Qiu, Z.W., Wang, H., Yan, Q.H., Li, S.S., Wang, L.M., Bu, A., Mu, S.L., Li, P., Wei, X.P., 2016. Zircon U-Pb geochronology and Lu–Hf isotopes of the quartz porphyry in the Changpu Sn polymetallic deposit, Guangdong Province, SE China and its geological significance. Geochemica 45, 374–386 (in Chinese with English abstract).
Qiu, Z.W., Yan, Q.H., Li, S.S., Wang, H., Tong, L.X., Zhang, R.Q., Wei, X.P., Li, P., Wang, L.M., Bu, A., Yan, L., 2017a. Highly fractionated Early Cretaceous I-type granites and related Sn polymetallic mineralization in the Jinkeng deposit, eastern Guangdong, SE China: constraints from geochronology, geochemistry, and Hf isotopes. Ore Geol. Rev. 88, 718–738.
Qiu, Z., Li, S., Yan, Q., Wang, H., Wei, X., Li, P., Wang, L.M., Bu, A., 2017b. Late Jurassic Sn metallogeny in eastern Guangdong, SE China coast: evidence from geochronology, geochemistry and Sr–Nd–Hf–S isotopes of the Dadaoshan Sn deposit. Ore Geol. Rev. 88, 63–83.
Rubatto, D., Gebauer, D., 2000. Use of cathodoluminescence for U-Pb zircon dating by ion microprobe: some examples from the Western Alps. In: Cathodoluminescence in Geosciences. Springer, Berlin Heidelberg, pp. 373–400.
Selby, D., Creaser, R.A., 2001. Re–Os geochronology and systematics in molybdenite from the Endako porphyry molybdenum deposit, British Columbia, Canada. Econ. Geol. 96, 197–204.
Shen, W., Yu, J., Zhao, L., Chen, Z., Lin, H., 2003. Nd isotopic characteristics of post-Archean sediments from the Eastern Nanling Range: evidence for crustal evolution. Chin. Sci. Bull. 48 (16), 1679–1685.
Shu, L.S., Zhou, X.M., Deng, P., Wang, B., Jiang, S.Y., Yu, J.H., Zhao, X.X., 2009. Mesozoic tectonic evolution of the Southeast China Block: new insights from basin analysis. J. Asian Earth Sci. 34 (3), 376–391.
Simon, A.C., Ripley, E.M., 2011. The role of magmatic sulfur in the formation of ore deposits. Rev. Mineral. Geochem. 73, 513–578.
Söderlund, U., Patchett, P.J., Vervoort, J.D., Isachsen, C.E., 2004. The 176Lu decay constant determined by Lu–Hf and U-Pb isotope systematics of Precambrian mafic intrusions. Earth Planet. Sci. Lett. 219, 311–324.
Stein, H.J., Markey, R.J., Morgan, J.W., Hannah, J.L., Scherstén, A., 2001. The remarkable Re–Os chronometer in molybdenite: how and why it works. Terra Nova 13, 479–486.
Sun, S.S., McDonough, W.E., 1989. Chemical and isotopic systematics of oceanic basalts: implications for mantle composition and processes. In: Saunders, A.D., Norry, M.J. (Eds.), Magmatism in the Ocean Basins. Geological Society of London. Special Publication 42, 313–345.
Sun, Y.L., Xu, P., Li, J., He, K., Chu, Z.Y., Wang, C.Y., 2010. A practical method for determination of molybdenite Re–Os age by inductively coupled plasma-mass spectrometry combined with Carius tube-HNO_3 digestion. Anal. Methods 2, 575–581.
Taylor, S.R., Mclennan, S.M., 1985. The Continental Crust: Its Composition and Evolution. Blackwell, London, pp. 1–312.
Wang, Y., Fan, W., Guo, F., Peng, T., Li, C., 2003. Geochemistry of Mesozoic mafic rocks adjacent to the Chenzhou-Linwu fault, South China: implications for the lithospheric boundary between the Yangtze and Cathaysia blocks. Int. Geol. Rev. 45, 263–286.
Wang, X., Mao, J., Cheng, Y., Liu, P., Zhang, X., 2016. Zircon u-pb age, geochemistry and hf isotopic compositions of quartzdiorite from the Xinliaodong Cu polymetallic deposit in eastern Guangdong Province. Geol. Bull. China 35 (8), 1357–1375.
Wei, G.J., Liang, X.R., Li, X.H., Liu, Y., 2002. Precise measurement of Sr isotopic composition of liquid and solid base using (LP)MC-ICPMS. Geochimica 31, 295–299.
Whalen, J.B., Currie, K.L., Chappell, B.W., 1987. A-type granites: geochemical characteristics, discrimination and petrogenesis. Contrib. Miner. Petrol. 95, 407–419.
Wong, J., Sun, M., Xing, G.F., Li, X.-H., Zhao, G.C., Wong, K., Yuan, C., Xia, X.P., Li, L.M., Wu, F.Y., 2009. Geochemical and zircon U-Pb and Hf isotopic study of the Baijuhuajian metaluminous A-type granite: extension at 125–100 Ma and its tectonic significance for South China. Lithos 112, 289–305.
Wu, Y.B., Zheng, Y.F., 2004. The genesis of zircon and the constraints on the interpretation of U-Pb age. Chin. Sci. Bull. 49 (16), 1589–1604 (in Chinese with English abstract).
Wu, F.Y., Jahn, B.M., Wilde, S.A., Lo, C.H., Yui, T.F., Lin, Q., Sun, D.Y., 2003. Highly fractionated I-type granites in NE China (I): geochronology and petrogenesis. Lithos 66, 241–273.
Wu, F.Y., Yang, Y.H., Xie, L.W., Yang, J.H., Xu, P., 2006. Hf isotopic compositions of the standard zircons and baddeleyites used in U-Pb geochronology. Chem. Geol. 234, 105–126.
Wu, S.H., Mao, J.W., Xie, G.Q., Geng, J.Z., Xiong, B.K., 2015. Geology, geochronology, and Hf isotope geochemistry of the Longtougang skarn and hydrothermal vein Cu–Zn deposit, North Wuyi area, southeastern China. Ore Geol. Rev. 70, 136–150.
Wyborn, D., Chappell, B.W., James, M., 2001. Examples of convective fractionation in high temperature granites from the Lachlan Fold Belt. Aust. J. Earth Sci. 48, 531–541.
Xia, X.H., 2009. A study of the volcano-hydrothermal genesis of the Guantian Cu-Fe-bearing pyrite deposit, Eastern Guangdong. Geological Rev. 45 (1), 823–828 (in Chinese with English abstract).
Xu, X.C., 1993. Geochemical studies on the Mesozoic magmatic and metallization, Eastern Guangdong Province (Ph.D. Thesis). Hefei University of Technology, Hefei, pp. 1–187 (in Chinese with English abstract).
Xu, X.C., Yue, S.C., 1999a. Source material and metallization of tin (tungsten, copper) polymetallic deposits in eastern Guangdong Province. J. Hefei Univ. Technol. 34 (1), 81–92 (in Chinese with English abstract).
Xu, X.C., Yue, S.C., 1999b. Continental crust anatexite: the genesis of Mesozoic granitic volcanic–intrusive complexes, eastern Guangdong Province—constraints on Pb–Nd–Sr multi-element isotopic systems. Geol. Rev. 45, 829–835 (in Chinese with English abstract).
Xu, X.C., Xie, Q.Q., Yue, S.C., 2000. Mesozoic volcanic and intrusive rocks in eastern Guangdong province, China: genesis, types and petrologic implication. Scientia Geologica Sinica 9 (3), 253–262.
Xu, X.S., O'Reilly, S.Y., Griffin, W.L., Wang, X.L., Pearson, N.J., He, Z.Y., 2007. The crust of Cathaysia: age, assembly and reworking of two terranes. Precambrian Res. 158, 51.
Xu, B., Jiang, S.Y., Luo, L., 2015. LA-MC-ICP-MS U-Pb dating of cassiterite from the Jianfengpo Sn deposit in the Pengshan Sn-polymetallic ore field, Jiangxi Province and its geological significance. Acta Petrologica Sinica 31 (3), 701–708.
Xu, B., Jiang, S.Y., Luo, L., Zhao, K.D., Ma, L., 2016. Origin of the granites and related Sn and Pb–Zn polymetallic ore deposits in the Pengshan district, Jiangxi Province, South China: constraints from geochronology, geochemistry, mineral chemistry, and Sr–Nd–Hf–Pb–S isotopes. Miner. Deposita 52 (3), 337–360.
Yang, S.Y., Jiang, S.Y., Zhao, K.D., Jiang, Y.H., Ling, H.F., Luo, L., 2012. Geochronology, geochemistry and tectonic significance of two Early Cretaceous A-type granites in the Gan-Hang Belt, Southeast China. Lithos 150, 155–170.
Zartman, R.E., Doe, B.R., 1981. Plumbotectonics: the model. Tectonophysics 75, 135–162.
Zhang, L.G., 1985. Hydrogen, oxygen, sulfur and carbon isotope geochemistry of the Lianhuashan porphyry type tungsten deposit. Mineral Deposits 4 (1), 54–63 (in Chinese with English abstract).
Zhang, W.L., Hua, R.M., Wang, R.C., Chen, P.R., Li, H.M., 2006. New dating of the Dajishan granite and related tungsten mineralization in southern Jiangxi. Acta Geol. Sinica 80, 956–962 (in Chinese with English abstract).
Zhang, Y.Q., Dong, S.W., Li, J.H., Cui, J.J., Shi, W., Su, J.B., Li, Y., 2012. The new progress in the study of Mesozoic tectonics of South China. Acta Geoscientica Sinica 33 (3), 257–279 (in Chinese with English abstract).
Zhang, G.W., Guo, A.L., Wang, Y.J., et al., 2013. Tectonics of South China continent and its implications. Sci. China Earth Sci. 56, 1804–1828 (in Chinese).
Zhang, Y., Yang, J.H., Sun, J.F., Zhang, J.H., Chen, J.Y., Li, X.H., 2015. Petrogenesis of Jurassic fractionated I-type granites in Southeast China: constraints from whole-rock geochemical and zircon U-Pb and Hf–O isotopes. J. Asian Earth Sci. 111, 268–283.
Zhao, X.L., Yu, M.G., Liu, K., Mao, J.R., Ye, H.M., Xing, G.F., 2012. The magmatic and genetic evolution of Early Cretaceous granitoids in eastern Guangdong Province. Geol. Rev. 58 (5), 965–977 (in Chinese with English abstract).
Zhou, X.M., Sun, T., Shen, W.Z., Shu, L.S., Niu, Y.L., 2006. Petrogenesis of Mesozoic granitoids and volcanic rocks in South China: a response to tectonic evolution. Episodes 29, 21–26.

Zhou, Z.M., Ma, C.Q., Xie, C.F., Wang, L.X., Liu, Y.Y., Liu, W., 2016. Genesis of highly fractionated I-type granites from Fengshun complex: implications to tectonic evolutions of South China. J. Earth Sci. 27, 444–460.
Zhu, W.G., Zhong, H., Li, X.H., He, D.F., Song, X.Y., Ren, T., Chen, Z.Q., Sun, H.S., Liao, J. Q., 2010. The early Jurassic mafic–ultramafic intrusion and A-type granite from northeastern Guangdong, SE China: age, origin, and tectonic significance. Lithos 119, 313–329.

Further reading

Li, X., Li, W., Li, Z.X., 2007a. On the genetic classification and tectonic implications of the Early Yanshanian granitoids in the Nanling Range, South China. Chin. Sci. Bull. 52 (14), 1873–1885.